Chem Soc Rev

Cite this: *Chem. Soc. Rev.*, 2012, **41**, 8140–8162

www.rsc.org/csr

CRITICAL REVIEW

Synthesis and catalysis of chemically reduced metal–metalloid amorphous alloys†

Yan Pei,[a] Gongbing Zhou,[a] Nguyen Luan,[b] Baoning Zong,*[c] Minghua Qiao*[a] and Franklin (Feng) Tao*[a]

Received 21st May 2012
DOI: 10.1039/c2cs35182j

Amorphous alloys structurally deviate from crystalline materials in that they possess unique short-range ordered and long-range disordered atomic arrangement. They are important catalytic materials due to their unique chemical and structural properties including broadly adjustable composition, structural homogeneity, and high concentration of coordinatively unsaturated sites. As chemically reduced metal–metalloid amorphous alloys exhibit excellent catalytic performance in applications such as efficient chemical production, energy conversion, and environmental remediation, there is an intense surge in interest in using them as catalytic materials. This *critical review* summarizes the progress in the study of the metal–metalloid amorphous alloy catalysts, mainly in recent decades, with special focus on their synthetic strategies and catalytic applications in petrochemical, fine chemical, energy, and environmental relevant reactions. The review is intended to be a valuable resource to researchers interested in these exciting catalytic materials. We concluded the review with some perspectives on the challenges and opportunities about the future developments of metal–metalloid amorphous alloy catalysts.

1. Introduction

Amorphous alloys are also referred to as non-crystalline alloys or metallic glasses. Noting that only in very few cases a single metal can be made into the amorphous form,[1] it is adequate to use the term "alloy" here. Amorphous alloys are intrinsically different from their crystalline counterparts in the arrangement of the constituting atoms. The atoms only have short-range ordering in amorphous alloys, while these short-range ordered structures (analogous to atomic clusters)[2] are linked randomly with each other, thus lacking the long-range ordered topological structure.[3] Short-range ordering means that the nearest interatomic distances and coordination numbers are constant. The extremely disordered atomic arrangement in long range renders amorphous alloys isotropic and homogeneous structure devoid of structural characteristics of crystalline

[a] *Department of Chemistry and the Shanghai Key Laboratory of Molecular Catalysis and Innovative Materials, Fudan University, Shanghai 200433, P. R. China. E-mail: mhqiao@fudan.edu.cn*
[b] *Department of Chemistry and Biochemistry, University of Notre Dame, Notre Dame, Indiana, USA 46556. E-mail: ftao@nd.edu*
[c] *State Key Laboratory of Catalytic Materials and Reaction Engineering, Research Institute of Petroleum Processing, Beijing 100083, P. R. China. E-mail: zongbn.ripp@sinopec.com*
† Part of the bimetallic nanocatalysts themed issue.

Yan Pei

Yan Pei completed her BSc in applied chemistry in 1998 at Nanjing University of Chemical Technology. In 2007 she obtained her PhD in Physical Chemistry in Prof. Kangnian Fan and Prof. Minghua Qiao's group at Fudan University. She is currently an assistant research fellow in the Department of Chemistry, Fudan University. Her research interest focuses on the synthesis and characterization of novel metal catalysts for selective hydrogenation.

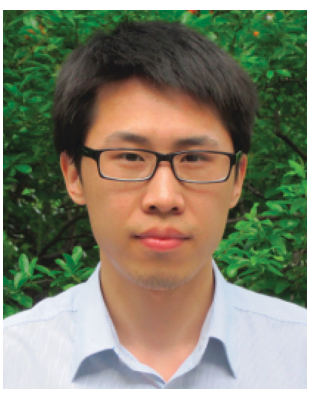

Gongbing Zhou

Gongbing Zhou received his BSc in applied chemistry from South China University of Technology in 2009. He is currently a PhD candidate at Fudan University, working under the supervision of Prof. Minghua Qiao. His current research effort concentrates mainly on the development of aromatics hydrogenation catalysts for cycloolefins production.

materials such as grain boundaries, dislocations, and stacking faults.[4] These structural peculiarities of amorphous alloys lead to unique mechanical and physical properties such as soft magnetism, high tensile strength and elasticity, and high corrosion resistance promising for a wide range of applications.[5]

In 1933, Zahn and Kramer pioneeringly discovered amorphous alloys *via* the evaporation–deposition technique.[6] However, it was not until 1980 that Smith *et al.* published their leading work on the catalytic application of amorphous alloys.[7] The successful preparation of Fe–Co–B amorphous alloy particles by reduction of metal ions with KBH_4 in aqueous solution by van Wonterghem *et al.* in 1986 greatly stimulated the blossom of amorphous alloys in catalysis, since the chemical reduction method is very convenient and much less demanding on the synthetic apparatus as compared to other techniques for the preparation of amorphous alloys, *e.g.*, the rapid quenching technique.[8] In fact, catalytic studies on amorphous alloys may be traced back to an earlier work of Brown and coworkers in 1953, who observed that Ni–B particles catalyzed H_2 production from aqueous $NaBH_4$,[9] although the amorphous structure was not recognized at that time.

According to Molnár *et al.*[10] and Baiker,[11] in principle, amorphous alloys have the following merits that justify them as high-performance catalytic materials:

(1) *Unlike crystalline alloys, the composition of the amorphous alloys can be adjusted in a wide range. The continuous control of the composition and the accompanying electronic property permit the fine tuning of the catalytic performance to meet the activity and/or selectivity demands.*

(2) *The isotropic and homogeneous characters of the amorphous alloys afford a uniform dispersion of active sites in a chemically identical environment, which is beneficial for the development of catalysts with high or exclusive selectivity.*

(3) *The high density of coordinatively unsaturated sites (CUSs) on amorphous alloys is important for heterogeneous catalysis, as the CUSs, similar to the low-coordination number step sites and kink sites on crystalline catalysts, are essential for the bonding and activation of the reactants, which ensures a high catalytic activity.*

Nguyen Luan

Nguyen Luan is a graduate student at Department of Chemistry and Biochemistry at University of Notre Dame. He works on preparation of bimetallic nanocatalysts and in situ and operando studies of surface chemistry and structure of nanocatalysts.

Baoning Zong

Baoning Zong received his BSc of Chemistry in 1985 from Peking University and his PhD of Chemical Engineering from the Research Institute of Petroleum Processing (RIPP) of Sinopec in 1991 under the supervision of Prof. Enze Min. He then joined RIPP, Sinopec. From 1995 to 1996, he worked as a post-doctoral fellow with Prof. G. Ertl at Fritz-Haber-Institute der Max-Plank-Gesellschaft. Since 1997, he has been a senior engineer of RIPP, Sinopec. He concentrated on catalytic applications and industrialization of amorphous metal alloys and magnetic stabilized bed reactor.

Minghua Qiao

Minghua Qiao received his BSc in Chemistry in 1994 and his PhD in 2000 from Fudan University, where he worked under the direction of Prof. Jingfa Deng. From 1997 to 1999, he temporarily studied in the Laboratory of Surface Chemistry led by Prof. Guoqin Xu at the National University of Singapore. In 2006, he became full professor for Physical Chemistry at Fudan University. His research concerns the design and characterization of amorphous alloys, skeletal alloys, metal–molecular sieve composite materials, and their applications in hydrogenation and energy-related catalysis.

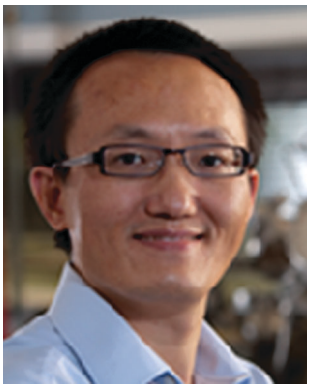

Franklin (Feng) Tao

Franklin (Feng) Tao joined Department of Chemistry and Biochemistry at University of Notre Dame as a tenure-track assistant professor in 2010 after obtaining a PhD in chemistry from Princeton University followed by a post-doctoral fellowship at Lawrence Berkeley National Lab and University of California at Berkeley. He is currently leading a research group interested in catalysis, energy science, and nano-science. He published about 70 research peer-reviewed articles in international journals and two books by Wiley. He serves on advisory board of Catalysis Science and Technology.

It is worthy of note that there are two other forms of metal catalysts that also hold the merits of amorphous alloy catalysts mentioned above. One is the so-called single-site metallic catalysts, *i.e.*, a single atom (or ion) functions as the active site of chemical turnover. Site-isolation is an essential characteristic of single-site catalysts. The other is nanocluster catalysts characterized by molecular aggregates between 2 and 30 atoms, as defined by Gates and coworkers[12] and Thomas.[13] As compared to amorphous alloys, the term "long-range" is virtually inapplicable to these metal catalysts bearing especially small dimension. More details about these novel catalysts and their promising applications can be found in reviews by Thomas and coworkers.[14–18]

In terms of the preparation of amorphous alloy catalysts, the rapid quenching method and the chemical reduction method mentioned above are two most frequently adopted means.[10,11,19–22] Since the rapid quenching method should ensure a cooling rate of at least 10^5–10^6 K s^{-1} in an inert atmosphere or *in vacuo*, it is technologically more challenging and costly for bench-scale preparation. The compositions of some amorphous alloys prepared by this method are limited by their high melting points. Thus sometimes only amorphous alloys with the ratio of different elements near the eutectic composition can be obtained. In this respect, the chemical reduction method is more versatile and economical.

The chemical reduction method involves the reduction of metal salt with reductants such as borohydride (BH_4^-) or hypophosphite ($H_2PO_2^-$) usually in an aqueous solution, producing metal–boride (M–B) or metal–phosphide (M–P) amorphous alloy particles.[8,23] The chemical reduction method can conveniently integrate with traditional catalyst preparation methods or new materials synthetic strategies. Preparation parameters such as temperature, pH, solvent, metal source, metal/reductant ratio, adding sequence, and adding speed strongly affect the composition and structure of the amorphous alloys,[24–31] thus providing abundant possibilities for the manipulation of the catalytic performance. Aside from binary M–B(P) amorphous alloys, amorphous alloys with one or more metals or metalloids can be readily prepared by using a mixed solution of metal salts or reductants.[23,32–36] Chemical reduction of metal ions adsorbed on supports leads to supported amorphous alloy catalysts.[22,37] The large surface area of the support can accommodate amorphous alloy nanoparticles in high dispersion, which greatly improves the utility of the active sites. Owing to the stabilization effect of the support as a heat sink, the supported amorphous alloy nanoparticles can retain their amorphous structure at temperatures higher than the unsupported counterparts, thus remarkably extending the applications and lifetime of the amorphous alloys in catalysis.[22] In addition, characters of supports such as porosity, acidity, and hydrophilicity offer additional means for the tailoring of the reaction pathway. All these features make amorphous alloys attractive materials in heterogeneous catalysis.

Several excellent reviews have been published on the advances in the catalysis on rapidly quenched[10,11,38] and chemically reduced amorphous alloy catalysts[21,22] in the last century. To distinguish from these reviews, our review will focus on research efforts mainly in the new century on chemically reduced metal–metalloid amorphous alloy catalysts. The fundamental aspects of the amorphous alloy catalysts, *i.e.*, structural and electronic properties, as well as promotion effects, will be addressed after introduction. Next, progress in the preparation strategies of amorphous alloy catalysts will be reviewed, with special emphasis on the designed synthesis of size-specific amorphous alloy nanoparticles, tailored assembly of amorphous alloys with novel morphologies, and new protocols for the supporting of amorphous alloys. Then, applications of the amorphous alloy catalysts in petrochemical, fine chemical, energy, and environment relevant reactions will be presented. Lastly, we will concisely discuss on some of the scientific challenges and opportunities in this field.

2. Basic physical aspects

2.1 Structural property

There are only few in-depth studies on the structural information of the metal–metalloid amorphous alloy catalysts.[39–42] In most cases, the amorphous structure is qualitatively determined by conventional characterization techniques such as X-ray diffraction (XRD), a combination of transmission electron microscopy (TEM) and selected area electron diffraction (SAED), and differential scanning calorimetry (DSC). For amorphous alloys, their XRD patterns are only characterized by a featureless broad peak. Under TEM observation, the chemically reduced amorphous alloy particles usually display spherical contour or irregularly shaped aggregates of spherical particles. In the SAED pattern, there is a diffractive halo, rather than distinct rings or dots characteristic of microcrystallites or single crystals, respectively. DSC reveals exothermic peak(s) due to the occurrence of structure transition and/or crystallization. These characterizations are unable to provide quantitative structural information of the amorphous alloys. Thus an accurate structure–performance relationship cannot be established. Although high-resolution TEM (HRTEM) is powerful in elucidating the microstructure of crystals, the high-energy electron beam of several hundreds of keVs is detrimental even to crystalline materials, not to mention the thermodynamically metastable amorphous alloys. So, we should be very careful when using this technique to investigate and interpret the microstructure of amorphous alloys.

As far as the short-range ordered and long-range disordered structure of the amorphous alloy is concerned, an extended X-ray absorption fine structure (EXAFS) technique is very suitable for its structural determination. Although neutron beam-based techniques are also powerful in structural analysis of amorphous alloys, these techniques are far less accessible. EXAFS measures the photo-absorption coefficient in the vicinity of the ionization edge of the element of choice, which is a unique probe for the revelation of the local atomic and electronic structure of absorbing centers.[43,44] EXAFS provides direct information on the local environment of a specific atom without the requirement of long-range ordered structure as required for XRD. Analysis of the EXAFS spectra allows for the extraction of bonding distances, number and type of

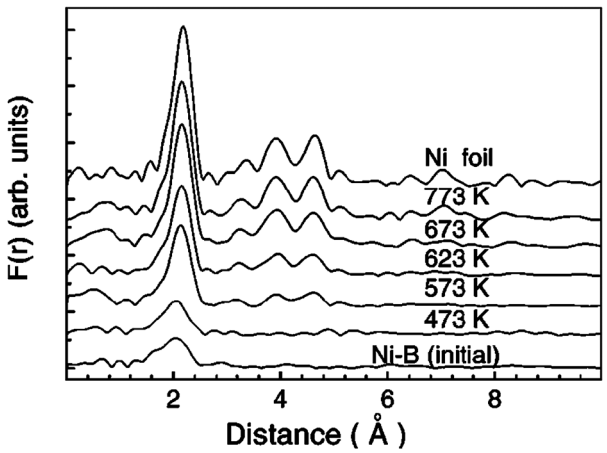

Fig. 1 Radial distribution functions of an ultrafine Ni–B amorphous alloy annealed at different temperatures. Reproduced from ref. 39 with kind permission from the American Physical Society.

neighboring atoms within the first few shells around the center atom, which are especially valuable for the interpretation of the microstructure of amorphous alloys. The major limitation of EXAFS is that it only provides structure-averaged information of the same absorber atoms. If absorber atoms adopt several configurations, individual local structural information cannot be obtained.

Fig. 1 shows the radial distribution functions (RDFs) of the as-prepared and thermally treated $Ni_{70}B_{30}$ samples, obtained from their $k^3\chi(k)$ by Fourier transform of the EXAFS spectra.[39] Only one prominent peak due to the first nearest neighbor of Ni atoms is observed for the as-prepared and 473 K-annealed samples, which unambiguously confirms their amorphous structure. In contrast, for crystalline Ni foil, aside from the intense first peak, there are distinct second and third nearest-neighbor peaks. By fitting the EXAFS spectra, the Ni–Ni and Ni–B distances and coordination numbers were determined. The Ni–Ni distance in the amorphous sample is much longer than that in the completely crystallized one. Considerable Ni–B coordination exists in the amorphous sample, while it is negligible in the completely crystallized sample.

By means of EXAFS, subtle structural difference between different amorphous alloys can be distinguished, which is unachievable by conventional techniques. For $Ni_{70}B_{30}$ prepared at various temperatures, Wei and coworkers revealed that the coordination geometry surrounding Ni atoms is a structure of amorphous Ni-like for the sample prepared at 273 K, suggesting that Ni and B atoms aggregated into Ni- and B-enriched clusters, respectively.[42] It is possible that only small fractions of B enter into the Ni cluster, and/or Ni and B atoms only interact at the interface between their respective clusters. $Ni_{70}B_{30}$ prepared at 313 K has amorphous Ni_3B-like structure with shorter first Ni–B coordination distance. These results indicate that the preparation temperature strongly affects the local structure of the $Ni_{70}B_{30}$ amorphous alloy.

The above finding on the microstructure of $Ni_{70}B_{30}$ prepared at 273 K is partly in line with the report of Geng *et al.*, which evidenced by HRTEM that their Ni–B nanoparticles prepared by chemical reduction are made up of tiny Ni nanoparticles (1–3 nm) embedded in a matrix of B-containing species.[45] It is noticed that the Ni nanoparticles in their Ni–B sample are crystalline, which may be caused by differences in the preparation conditions. It should be stressed that chemical reduction does not always lead to amorphous structure. For example, when copper salt was reduced by KBH_4, Cu crystallites were obtained.[46–48] When the pH of the solution for the preparation of the Ni–P alloy was 8.1 or lower, reflections assignable to *fcc* Ni emerged.[31]

With the aid of EXAFS, the structure–performance relationship can be described at a more microscopic level. Wei and coworkers studied the effect of annealing temperature on the structure of nano-amorphous Ni–B and the benzene hydrogenation activity.[40] It was found that below 573 K, Ni–B samples retained their original amorphous structure. At 573 K and 623 K, the nano-amorphous Ni–B was crystallized into nano-crystalline Ni and crystalline Ni_3B. At 773 K, crystalline Ni_3B was decomposed to crystalline Ni, and nano-crystalline Ni aggregated into large Ni grains. Combined with the temperature-dependent intrinsic activity, the catalytic activity of various Ni phases in benzene hydrogenation is ranked as nano-crystalline Ni > nano-amorphous Ni–B alloy > crystalline Ni ≈ crystalline Ni_3B.

X-ray absorption near-edge structure (XANES) is also powerful in providing electronic and geometric information. Qiao and coworkers observed that with the increment of the amount of Fe in the Co–B amorphous alloy, the Co *K*-edge XANES spectra remained identical, but in sharp difference from that of the Co foil (Fig. 2).[41] The close resemblance of the Co *K*-edge XANES spectra, along with the virtually unchanged structural parameters derived from EXAFS, strongly indicates that the metal atoms in Co–B and Co–Fe–B amorphous alloys have identical local symmetry. Thus, the intensity of the pre-edge peak in Fig. 2 can be taken as a measure of the occupation degree of the 3d holes. According to the figure,

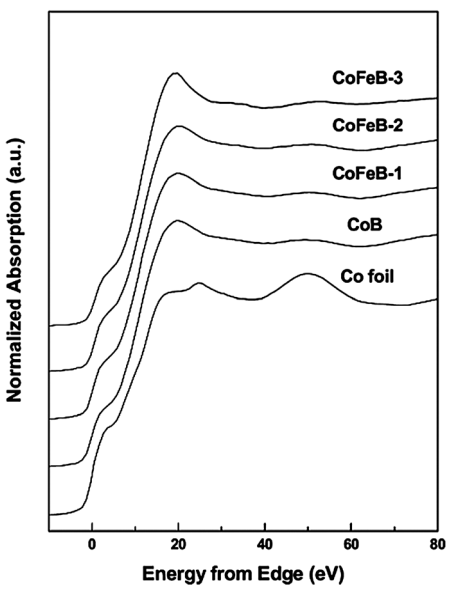

Fig. 2 Normalized Co *K*-edge XANES spectra for the Co foil and the Co–B and Co–Fe–B catalysts. Reproduced from ref. 41 with kind permission from Elsevier.

Co in these amorphous alloys has similar 3d population irrespective of the Fe content. Thus, the influence of Fe on the Co–B amorphous alloy was attributed to the geometrical effect, rather than the electronic effect.

2.2 Electronic property

Metal–metalloid amorphous alloys exhibit high catalytic activity and/or selectivity in a large collection of reactions. Reaction rates faster than typical rates on RANEY® Ni or comparable to those on noble metal catalysts have been reported.[49–55] A rational interpretation of the mechanism responsible for the enhanced catalytic performance of the amorphous alloys requires not only a clarification of the microstructure, but also an understanding of the electronic property.

It is interesting that photoelectron spectroscopic investigations suggest that the electronic effects of B or P alloying with Ni are at variance, though both metalloids are more electronegative than Ni. For a Ni–B amorphous alloy, there is a consensus that B displays a positive binding energy (BE) shift,[56–60] which is interpreted as electron donation from B to Ni[56–59] or to oxygen species left in the alloy.[21,60] For a Ni–P amorphous alloy, the situation is more complicated. Negative BE shift,[21,56,57,60] no significant BE shift,[61] and composition-dependent BE shift of P[58,59] have been documented. Imanaka and Tamaki found that P displayed positive BE shift for Ni–P alloys containing $\geq 75\%$ of Ni, while negative BE shift for alloys with lower Ni content.[58,59] To eliminate the possible interferences of the charging effect and spectrometer work-function on the BE shifts, under strictly defined characterization conditions, Deng and coworkers verified that B showed positive BE shift relative to elemental B in the Ni–B amorphous alloy, P displayed no detectable BE change relative to elemental P for the Ni–P amorphous alloy with surface composition of $Ni_{76}P_{24}$, and Ni in both alloys showed no BE shift relative to Ni foil.[62] Based on the positive BE shift of B for the Ni–B amorphous alloy, Okamoto *et al.* claimed that B donated electrons to the alloying Ni.[56,57] The charge transfer may be evidence of the bonding between Ni and B in the amorphous alloy, which leads to a smaller Ni–B atomic distance than the summation of Goldschmidt radii of individual atoms as determined by EXAFS,[63] as also observed on the Co–B amorphous alloy.[41]

The invariant Ni 2p BE of Ni after alloying with B may be justified by the following argument.[64] From Ni^0 to Ni^{2+}, the Ni 2p BE shift is *ca.* +1 eV, while from B^0 to B^{3+}, the B 1s BE shift is *ca.* +6 eV. By considering the B 1s BE shift of +1.1 eV in the Ni–B amorphous alloy, along with the surface composition of $\sim Ni_{75}B_{25}$, an estimation gave a Ni 2p BE shift of −0.06 eV ($\Delta BE = -(1.1 \times 0.25)/(6 \times 0.75)$), which is well within the detection error of ±0.2 eV on a conventional XPS spectrometer. This argument can analogously explain the apparently unchanged BEs of Co 2p, Fe 2p,[41] and Ru 3d levels[65] in M–B amorphous alloys. Actually, Diplas *et al.* observed the slight negative BE shifts of the Ni 2p and 3p levels of Ni–B amorphous alloys containing 30 at% and 50 at% of B at improved energy resolution.[66] Based on Auger parameter measurements and primary and secondary features of the XPS spectra, they proved that the positive BE shift of B is not caused by the final state effect, but rather by electron donation from B to Ni. The seemingly contradiction between the direction of electron transfer and the electronegativity sequence of Ni and B is rationalized by considering the increase in the electron density at the Ni sites in the Ni–B amorphous alloys to be a result of shortening of the interatomic distances *via* the formation of hybridized bonds between Ni and B atoms.[66] In a successive work, the authors extended this conclusion to Ni–P and Ni–S systems, and suggested that the Ni sites experiencing a higher electron density in the Ni–X (X = B, S, P) amorphous alloys than in pure Ni could be the reason for the increased catalytic activity.[67] Moreover, using density function theory (DFT) calculations, Diplas and Løvvik found that the Ni 3d density of state (DOS) of the Ni–B, Ni–P, and Ni–S alloys shows strong similarity to that of Pt, which may account for their high activity in H_2 evolution reaction.[68] However, it should be cautious that their periodic models may not be adequate to represent the geometric structure of amorphous alloys.

Since amorphous alloys lack long-range ordered structure and can be looked as a stacking of metal–metalloid atomic clusters with short-range ordering,[3] a cluster model seems to be a proper choice to represent the local structure of amorphous alloys. As experiments have indicated the presence of direct B–B contact in M–B amorphous alloys[69] and the absence of direct P–P contact in M–P amorphous alloys,[70] Fan and coworkers constructed M_mB_2 and M_nP (M = Ni, Co) cluster models and calculated their geometric and electronic properties using DFT.[71–74] Electron donation from B to Ni or Co and electron donation from Ni or Co to P were demonstrated by their theoretical simulations. For $TiO_2(110)$ surface-supported Co_2B_2 or $NiFeB_2$ clusters, DFT calculations similarly gave the direction of electron donation from B to metals.[75,76] Using Ni_nP (n = 1–6) cluster models, the experimentally observed inverse of the direction of electron donation between Ni and P[58,59] was nicely reproduced at $n = 6$.[72]

2.3 Promotion effect

Inclusion of metal promoter(s) in metal–metalloid amorphous alloy catalysts can optimize the catalytic performance by affecting the structural and/or electronic characteristics. Promoters are generally present in the oxidized state and/or metallic state, depending on their reducibility and alloying ability.[77] When the promoter is in the oxidized state, *e.g.*, early transition metal, it generally promotes the dispersion of the amorphous alloy by inhibiting the agglomeration of the nanoparticles and improves the active surface area. The acidic property of oxidized metal species is favorable for the adsorption and activation of polar groups, such as carbonyl groups and nitro groups. When the promoter is in the metallic state, *e.g.*, late transition metal, it not only stabilizes the amorphous structure, but also forms chemical bonds with the constituting atoms of the amorphous alloy, which tune the electron population at the Fermi level.[78] Furthermore, the promoter may change the composition of the M–B amorphous alloy,[51,79] which affects the local structure and electronic property of M alloying with B.

For instance, Mo and Ce have been used as promoters for Co–B[80] and Ni–B catalysts.[81,82] These promoters, in the form

of MoO_3 and CeO_2, not only accelerated the reaction rate, but also elevated the crystallization temperature (T_c). The Cr promoter in the Ni–B catalyst, most likely in the form of Cr_2O_3, functioned as participants between Ni–B nanoparticles, thus enhancing the dispersion of the active sites, and as Lewis acid sites that can lower the π^*_{CO} orbital of the reactant, thus directing a carbonyl group-bonded configuration.[83] Addition of Sn to the Ru–B/γ-Al_2O_3 catalyst not only improves the dispersion and thermal stability significantly, but also increases the B/Ru ratio, the electron density of Ru, and the adsorption strength of H_2.[84] Promotion of the Ni–B nanocatalyst with W or Mo caused an increment of the B content associated with Ni, which thus altered the hydrogenation activity.[79]

The promotion effect of metallic Co on the Ni–B amorphous alloy was interpreted both electronically and structurally. Co donates electron to Ni, leading to electron-enriched Ni and electron-deficient Co.[34,85] The structural disorder of the Ni–Co–B catalyst increases with the content of metallic Co.[78] The promotion effect of metallic Fe has been studied on Ni–B[86] and Ni–P catalysts.[87] The promotion effect of Fe was attributed to electron donation from metallic Fe to Ni, which is favorable for the activation and hydrogenation of polar groups. Incorporation of Fe into the Co–B catalyst favored the hydrogenation of carbonyl groups *via* the ensemble size effect.[41] Although the oxidation state of La was not specified, the effect of La on the Ni–B catalyst was interpreted as electronic modification of Ni by La.[51] It is acknowledged that the change in the electron density at the Fermi level can affect the dissociative chemisorption of H_2, which will influence the hydrogenation activity in reactions where H_2 dissociation is the rate-determining step (rds).[78,88,89]

3. Synthesis of metal–metalloid amorphous alloy catalysts with well defined morphologies

3.1 Monodispersed nanoparticles

The chemical reduction method has been most frequently adopted to synthesize nanosized amorphous alloy catalysts. Conventionally, the reduction is performed by adding a solution containing the chemical reductant to a solution containing the metal salt or *vice versa*, at a certain temperature under stirring. The vigorous and exothermic reduction reaction may induce severe agglomeration or aggregation of the nanoparticles, thereby lowering the catalytic efficiency. To remove the disadvantage of conventional chemical reduction methods, various preparative strategies to uniform amorphous alloy nanoparticles have been developed, including the microemulsion method,[53,90,91] polymer stabilization,[92–94] and sonochemical technique.[95–99]

3.1.1 Microemulsion method. Microemulsion solutions are transparent, isotropic liquid media with nanosized water (oil) droplets dispersed in a continuous oil (water) phase and stabilized by surfactant molecules at the water/oil interface. The microemulsion method is suitable for the preparation of uniform particles with controllable sizes and morphologies. Surfactant-covered liquid droplets can function as micro- or nano-reactors providing a homogeneous microenvironment for the formation of nanoparticles. The surfactant may adsorb on the nanoparticle surface when the particle size approaches that of the liquid droplet, acting as a protective agent to stabilize and restrict the size of the nanoparticles. Liaw and coworkers prepared surfactant-stabilized Ni–B catalysts (ME-NiB) in a ternary microemulsion system of water–cetyl-trimethyl-ammonium bromide (CTAB)–*n*-hexanol.[53] It was found that the particle sizes of the ME-NiB were not fully dominated by the size of the water-in-oil (W/O) reverse microemulsion droplets. They were also influenced by the composition of the microemulsion, the concentration of the Ni salt, the amount and the addition speed of $NaBH_4$, and the temperature. The particle size and size distribution of the ME-NiB were substantially reduced and narrowed to 3–8 nm, as compared to the size (20–50 nm) of conventional Ni–B nanoparticles (Fig. 3). In a similar approach, Wu and coworkers synthesized spherical and rod-like Fe–B alloys in pseudo-ternary W/O microemulsions.[91] The particle size was mainly determined by the size of the microemulsion droplets, and the key factor affecting the morphology (spherical or rod-like) of the Fe–B nanoparticles was the interfacial property relevant to the *n*-butanol/CTAB ratio.

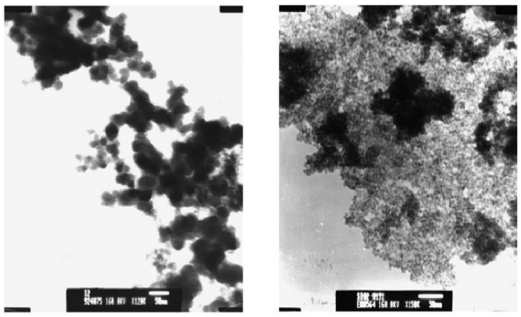

Fig. 3 TEM micrographs of NiB (left) and ME-NiB (0.15 M) (right) catalysts. Reproduced from ref. 53 with kind permission from Elsevier.

Synthesis in W/O microemulsions has limitations of low concentration of the product and environmental pollution. Li and coworkers designed an oil-in-water (O/W) microemulsion system comprising cyclohexane, polyethylene glycol (PEG), and water for the fabrication of uniform Co–B nanoparticles in large quantities.[90] Uniform Co–B nanoparticles with controllable particle sizes from 6 to 20 nm were synthesized by adjusting the cyclohexane content.

3.1.2 Polymer stabilization. The polymer stabilization method, which takes advantage of surface modification by the polymer molecules, is effective in improving the dispersion and stability of the nanoparticles. The reactive surfaces of the nanoparticles can be saturated with functionalized polymer molecules immediately after nucleation at multiple sites through the functional groups of the polymer, thus sterically preventing the agglomeration of the nanoparticles.[100,101]

Liaw and coworkers used water-soluble polyvinylpyrrolidone (PVP) as a capping agent to prepare the PVP-stabilized Ni–B and Co–Ni–B catalysts.[92,94] The molecular weight of PVP and the PVP/metal ratio in the salt solution affected the particle size and distribution of the nanoparticles. The particle size and distribution of PVP–Ni–B were decreased and

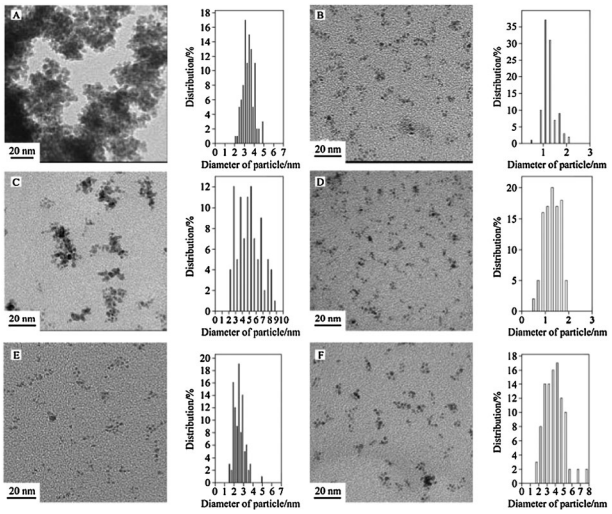

Fig. 4 TEM images (left) and the corresponding particle size distribution histograms (right) of the PVP-stabilized Ru–B colloids. Reproduced from ref. 93.

narrowed to 3–5 nm under optimal preparation conditions, which was about one-tenth of that of Ni–B without PVP protection.[94] Moreover, PVP–Ni–B was more stable than conventional Ni–B at temperatures above 573 K, despite the much smaller particle size of the former. Similar results were observed on the PVP–Co–Ni–B catalyst.[92] Bu *et al.* prepared a series of PVP-stabilized Ru–B colloidal catalysts in the range of 1.3–3.9 nm with sharp size distribution (Fig. 4).[93] The stirring time for mixing PVP and $RuCl_3$ and after KBH_4 addition, the Ru/PVP ratio, and the $RuCl_3$ concentration influenced the size of the Ru–B colloidal particles.

3.1.3 Ultrasound-assisted reduction. The ultrasound-assisted chemical reduction method has been proven to be effective in preparing amorphous alloys with homogeneous particle size. Ultrasonication can induce chemical reaction and inhibit particle aggregation due to acoustic cavitation, which produces unusual chemical environments.[102–107] Generally, the particle size can be controlled by adjusting the ultrasonication power[96–98] or time.[95,96] The effect of ultrasonication on the particle size is very pronounced for the Ru–B nanoparticles.[98] The conventional Ru–B nanoparticles displayed irregular, broadly distributed particles from 15–50 nm. In sharp contrast, the ultrasound-assisted reduction gave rise to monodispersed and spherical Ru–B nanoparticles with a much smaller size of 2.4–4.9 nm.

Besides the advantageous effect on reducing the particle size, the ultrasound-assisted method can induce a higher surface elemental B/M ratio. The improvement of the surface B/M ratio was identified on Co–B,[96] Ni–B,[97] and Ru–B nanoparticles[98] reduced under ultrasonication. The increased surface B content can invoke a stronger electronic interaction with M and higher thermal stability by impeding the migration of the metal atoms.

3.2 Special morphology

Nearly all metal–metalloid amorphous alloys prepared by conventional chemical reduction methods are present in the form of nonporous spherical nanoparticles due to their isotropic nature. In order to achieve high utility of the active species, a usual practice is to reduce the particle size to as small as possible. However, this may evoke separation problems as well as severe agglomeration. Inspired by natural materials with fascinating functions and enhanced properties associated with their unique shape and/or morphology, synthesis of materials with controlled texture and morphology is drawing more and more attention.[108,109] When used as catalysts, materials with special morphology may offer some advantages over their solid counterparts in terms of improved surface accessibility, easy recovery, and reduced cost.[110] Thus, a combination of the amorphous structure and new morphology is expected to lead to amorphous alloys with enhanced catalytic properties.

3.2.1 Hollow morphology. The hard-templating method has been most frequently used to fabricate amorphous alloys with special nanostructures, because of its advantage in transcriptive imprinting of the template morphology. By electroless plating of the desired amorphous alloy on the shape-decisive hard template, various amorphous alloys with hollow structures have been synthesized, including Ni–B[111] and Ni–P hollow microspheres,[112,113] and Co–Ni–P hollow rods.[114] This synthetic strategy usually involves three steps as shown in Scheme 1.[111] Firstly, the surface of the hard template is activated to facilitate the deposition of the amorphous alloy. Secondly, the amorphous alloy is deposited on hard templates, such as polystyrene (PS) microspheres,[111,113] hollow glass microspheres,[112] or *Bacillus*, a kind of rod-shaped bacteria,[114] to form core–shell structure through electroless plating. Finally, the core is removed by dissolution[111,113] or thermal annealing[114] to obtain the hollow structures (Fig. 5). We should be cautious that thermal annealing might be harmful to the amorphous structure.[114] It is easy to control the morphology and diameter of the amorphous alloy hollow materials by using templates of different morphologies and dimensions. The thickness of the amorphous alloy shell is adjustable by varying the plating time[111,112] or the concentration of the reductant.[111] The plating time and the pH of the plating solution also influence the quality of the amorphous alloy shell.[113]

Fabrication of hollow amorphous alloy materials through the soft-templating strategy led to Ni–B hollow spheres,[115] Fe–B, Co–B, Ni–B,[116] Ni–P–B, Ni–Cu–B, and Ni–Co–B hollow nanotubes.[117] The formation of Ni–B hollow spheres

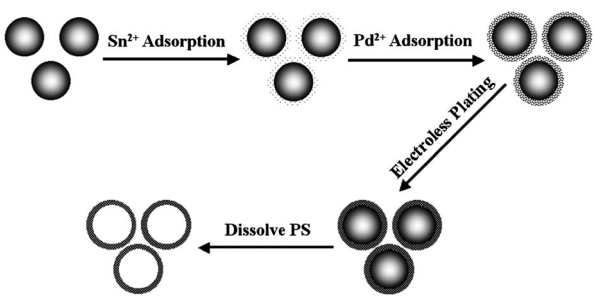

Scheme 1 Schematic outline of the steps involved in the fabrication of amorphous Ni–B hollow spheres. Reproduced from ref. 111.

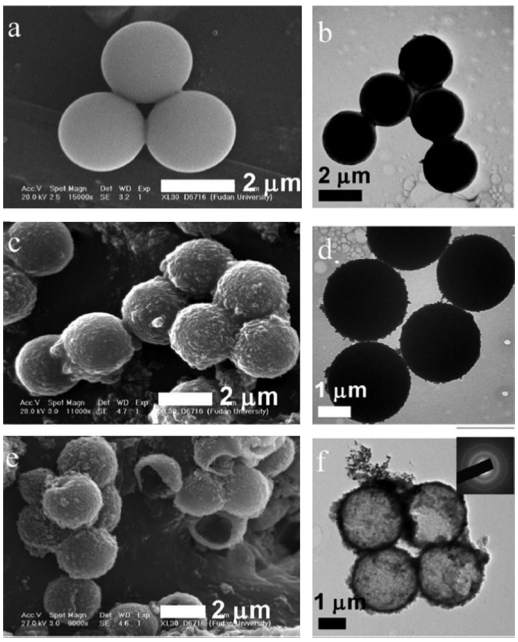

Fig. 5 SEM (a, c and e) and TEM (b, d and f) micrographs of the PS microspheres before and after Ni–B deposition: (a and b) pristine PS microspheres; (c and d) core–shell Ni–B–PS composites; (e, f) Ni–B hollow spheres. Inset shows the SAED pattern of the Ni–B hollow spheres. Reproduced from ref. 111.

is based on the emulsion droplets formed by the water–PEG–cyclohexylamine system, which provides an *in situ* template for the deposition of the Ni–B amorphous alloy.[115] The average cavity size of the product is almost the same as the diameter of the microemulsion droplet template.

Ding and coworkers synthesized Fe–B, Co–B, and Ni–B nanotubes with uniform size by using lyotropic non-ionic–anionic mixed surfactants as a template.[116] For example, the Fe–B nanotubes they synthesized are several micrometers long and have inner and outer diameters of *ca.* 50–55 and 60–65 nm, respectively (Fig. 6). By introducing P-, Co-, and Cu-containing compounds during the preparation, ternary Ni–P–B, Ni–Co–B, and Ni–Cu–B nanotubes were obtained.[117] These authors proposed that the presence of the lyotropic liquid crystals (LCs) was the key for the formation of the amorphous alloy nanotubes. During the reduction of metal ions located in the layer structure of the LCs, the released H_2 results in the cleavage and curling of the layered structure, leading to the formation of nanotubes.

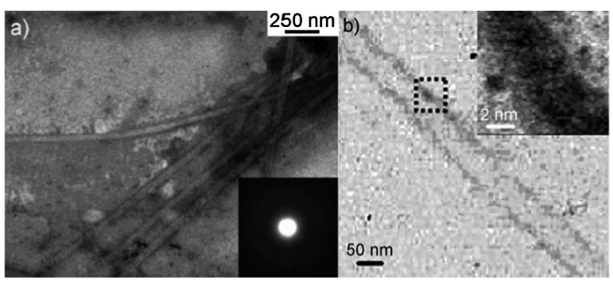

Fig. 6 (a) TEM image (80 kV) of Fe–B nanotubes; inset: the corresponding SAED pattern; (b) HRTEM image (200 kV) of one isolated Fe–B nanotube inset: expansion of marked section. Reproduced from ref. 116 with kind permission from Wiley-VCH.

3.2.2 Mesoporous texture. Mesoporous amorphous alloys represent a new trend towards the design of amorphous alloys with high surface area and large and uniform pore channels, which are attractive in catalytic applications. The mesopores facilitate a facile access of the guest molecules to the active sites, showing promise for an improved catalytic performance.[118,119] It has long been remained a great challenge to synthesize mesoporous amorphous alloys through surfactant self-assembly, since the surfactant-templated mesoporous structure is fragile to the vigorous and strongly exothermic reaction between the metal ions and the reductant.

Some strategies have been proposed to withhold the regular LC mesophases during chemical reduction. Successful endeavors include adding antifoaming agents, using metal salts in which anions have strong affinity to the cations, and selecting surfactants that can adsorb metal cations or BH_4^- to smooth the reduction process.[120,121] Worm-like mesoporous Ni–B,[122] Co–B,[120,123,124] and Ru–B[121] have been synthesized (Scheme 2). Furthermore, Li and coworkers synthesized mesoporous Fe–B, Co–B, Ni–B, and Ni–Co–B microspheres with tunable chamber size *via* co-templating from syringe-squeezing and surfactant self-assembly.[125] In this approach, yolk-shell structured Ni–B microspheres with an average diameter of *ca.* 200 nm were successfully synthesized. The formation mechanism was proposed as the establishment of the integrated outer shell and the ectoentad stepwise reduction of the Ni^{2+} ions inside the droplet. The mesoporous amorphous alloys prepared by the soft-templating strategy were of poor ordering degree. Only worm-like rather than regular mesopores have been constructed, since the measures mentioned above are still insufficient to completely suppress the damage of the LC mesophase by the drastic reduction process.

Nanocasting using mesoporous silica as a hard template is one of the most common strategies to fabricate crystalline materials with regular mesostructures.[126,127] Using the ultrasound-assisted reductant infiltration strategy, Chen *et al.* synthesized Ni–B nanoarray replicated from mesoporous siliceous SBA-15.[128] The silica-free Ni–B nanoarray is constructed by hexagonally packed nanowires with a uniform diameter of *ca.* 5 nm. These nanowires are interconnected by thinner Ni–B wires originating from the micropores within the wall of SBA-15,[119] thus ensuring the integrated structure of the Ni–B nanoarray after hard template removal.

3.2.3 Other morphologies. Amorphous alloys with chain-like,[129] rod-like,[129,130] and thin film[131,132] morphologies have

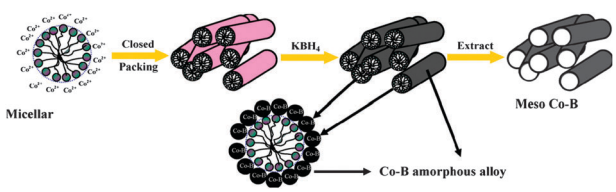

Scheme 2 Schematic illustration of the formation of mesoporous structure in Co–B amorphous alloy particles. Reproduced from ref. 120 with kind permission from Elsevier.

been reported in the literature. Chain- and rod-like Co–B nanomaterials were prepared by chemical reduction in CTAB and PVP aqueous solutions, respectively.[129] The chain-like Co–B was constructed by spherical particles connected one-by-one with nanoflakes on the particle surface. The rod-like Co–B was *ca.* 5 μm in length and 1 μm in diameter, with a porous structure formed by interlaced nanowires. Li and coworkers prepared chain-like Co–B by chemical reduction of Co^{2+} ions in a dodecanethiol–water biphasic system based on spontaneous self-assembly.[133] Dodecanethiol is essential for the formation of Co–B nanochains, which generates a biphasic system with aqueous solution and induces dipoles on Co–B nanoparticles. Rod-like Fe–B was prepared using anodic aluminum oxide (AAO) as the template.[130] The Fe–B nanoparticles were self-assembled within the uniform channels of AAO. By varying the duration of preparation, sphere- or rod-shaped Fe–B nanomaterials were obtained.

Patel and coworkers synthesized Co–B nanoparticle-assembled thin films with an average roughness of ~264 nm using pulsed laser deposition (PLD).[131,132] The peculiarities of the Co–B nanoparticles produced by PLD were related to their well-defined spherical shape and to their high particle density distribution free from coalescence, a deleterious process inhibiting the favorable surface/volume ratio that is critical to the catalysis process.[132] The Co–B film catalyst is easy to recover, and hence can be used to control the on–off of H_2 generation by catalytic decomposition of $NaBH_4$ and NH_3BH_3, which is a difficult task for Co–B nanoparticles.

4. Synthesis of supported metal–metalloid amorphous alloy catalysts

4.1 Synthetic strategy

In comparison with unsupported nanosized amorphous alloy catalysts, supported amorphous alloy catalysts not only permit easy product separation and catalyst recycle, but also generally possess improved catalytic efficiency and thermal stability owing to the attractive characters of the support.[37,82] Many endeavors have been devoted to the preparation of supported amorphous alloy catalysts. The conventional method involves impregnation of the support by metal salt solution for a certain period, followed by drying at above 373 K, and then subjected to chemical reduction. This method has limitations of loss of the active species during chemical reduction and reaction, severe agglomeration of the amorphous alloy nanoparticles, and weak metal–support interaction.

4.1.1 Modified drying process. Since the drying process is essential to the distribution of the metal cations on the support and hence the dispersion of the active species after reduction, modified drying methods, including two-step drying approach[64] and microwave heating,[134,135] have been proposed. Deng and coworkers developed the two-step drying approach for the preparation of Ni–B/γ-Al_2O_3.[64] As compared to the one-step drying approach, the two-step drying approach led to higher Ni–B dispersion and higher thermal stability, attributable to the better distribution of the metal ions on γ-Al_2O_3 during the modified drying process.

Microwave heating has attracted much attention in catalyst preparation due to its rapid and even heating ability leading to uniform distribution of the active species on the support.[136] It is found that microwave heating did not alter the composition, electronic property, and intrinsic catalytic activity of Ni–B/SiO_2, but led to smaller particle size, higher dispersion, and better thermal stability.[134]

4.1.2 Reductant impregnation. Different from catalysts reduced by H_2, the chemical reduction method opens the avenue to load the reductant on the support first, *i.e.*, the reductant-impregnation method. As compared to the conventional metal salt-impregnation approach, the reductant-impregnation method can lead to amorphous alloy catalysts with different composition and structure.[137–139] The Ni–B/AC catalyst prepared in this reversed impregnation sequence has larger surface area and porosity than that prepared in the conventional sequence,[139] which was also observed when using SiO_2 and Al_2O_3 as supports,[137,138] suggesting that it is a common phenomenon only related to the impregnation sequence. The reductant-impregnation method is also crucial for the successful preparation of silica sol-dispersed Ni–B nanoclusters, since gelation readily took place when $Ni(OAc)_2$ was mixed with the silica sol first.[140] Using the reductant-impregnation method, the Ni–B nanoclusters are homogenously dispersed with a particle size of only 1–2 nm on the silica surface.

4.1.3 Wetness reduction/deposition. Wang *et al.* employed the chemical deposition method and the impregnation–wetness–reduction method for the preparation of Ni–B/TiO_2 catalysts.[141] The former involves the reduction of a mixture of metal salt solution and support by the reductant. The latter cancels the drying step as compared to the conventional method. Most of the Ni^{2+} ions in the solution were carried over to TiO_2 by the former, while the Ni loading was only about one half of the nominal value by the latter, implying that only the strongly adsorbed Ni^{2+} ions can survive in this approach. On both catalysts, the half-spherical particle shape implies that the Ni–B nanoparticles bound tightly with TiO_2. The strong interaction between the highly dispersed Ni–B nanoparticles and TiO_2 accounts for the improved thermal stability of these catalysts.

4.1.4 Electroless plating. Electroless plating is a well-established technique for the fabrication of amorphous alloy coatings.[142] Electroless plating is characterized by a surface activation step and a plating solution containing stabilizer(s) to avoid its autogeneous decomposition. Zhang and coworkers investigated the preparation parameters of the Ni–B/MgO catalysts by Ag-activated electroless plating.[135,143,144] The size, composition, and loading of the Ni–B nanoparticles depended on the starting ethylenediamine(EN)/Ni^{2+} ratio and pH. The Ni–B particle size increased monotonically from ~16 to 35 nm when the pH increased from 12.4 to 13.6. Higher EN/Ni^{2+} ratio and pH led to higher Ni content in Ni–B. Addition of stabilizers to the plating solution changed the texture of the Ni–B particles from porous to solid.[143] Electroless plating under microwave irradiation increased the particle size, Ni loading, and B content of the Ni–B/MgO catalysts.[135]

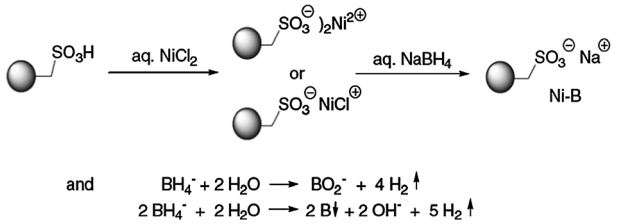

Scheme 3 Preparation of polymer-supported nanoamorphous Ni–B particles. Reproduced from ref. 145 with kind permission from Springer Science.

4.1.5 Ion exchange. Ion exchange followed by chemical reduction is effective in the preparation of cationic exchange resin-supported amorphous alloy catalysts (Scheme 3). Using this strategy, Wen and coworkers obtained polymer-supported Ni–B nanoparticles with adjustable Ni loadings and low degree of agglomeration.[145] After one ion exchange–reduction cycle, the Ni loading was 53.5 wt%. The loading was increased to 74.5 wt% after the second cycle. After several exchanges until the solution being almost neutral, the Ni loading reached as high as 93.2 wt%. The Ni–B particles were 60–70 nm in size and distributed evenly on the polymer surface. Such a high Ni loading has not been observed on SiO_2, Al_2O_3, AC, and TiO_2.[146]

4.1.6 *In situ* reduction. Reduction of unsaturated groups by borohydride in the presence a transition metal salt has long been documented.[147] During the reaction, the M–B particles are formed *in situ* as the catalyst. Caddick *et al.* used *in situ* generated Ni–B particles to promote the reduction of nitriles.[148] Rahman and Jonnalagadda modified this reaction protocol by adding SiO_2-supported $Ni(NO_3)_2$ instead of individual nickel salt to the reaction system containing $NaBH_4$.[149,150] The Ni–B/SiO_2 catalyst was formed *in situ* by $NaBH_4$ reduction of $Ni(NO_3)_2/SiO_2$. The Ni–B particles are tightly bound to the SiO_2 surface, as there was no leaching of the metal in the filtrate.

4.2 Mesoporous support

Regular mesoporous materials have shown great potential in catalysis, which is closely related to their specific features such as extremely high surface area and narrow pore size distribution. Their large channels allow diffusion of bulky compounds and present different types of shape selectivity such as reactant, product, and transition state.[151] These merits offer possibilities for obtaining highly dispersed amorphous alloy catalysts with better utilization of the active sites. The additional advantage of the improved dispersion is the reduced probability of agglomeration and thus, enhanced stability.[152–155]

It is expected that the size of the supported M–B amorphous alloy particles is closely related to their location on the mesoporous support. The uniform mesopore channels can confine the growth of the particles, leading to smaller particle size and more homogeneous particle size distribution, while the external surface does not have such a confinement effect. However, it was found that only SBA-15 can effectively accommodate amorphous alloy nanoparticles.[153–155]

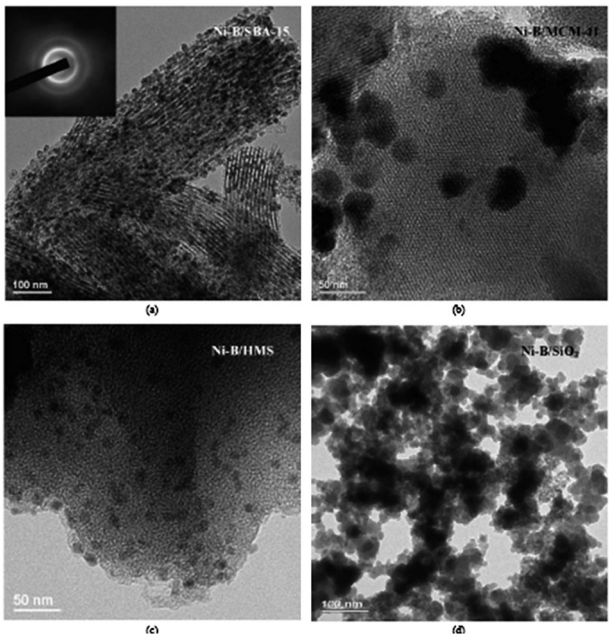

Fig. 7 TEM images of (a) Ni–B/SBA-15, (b) Ni–B/MCM-41, (c) Ni–B/HMS, and (d) Ni–B/SiO_2 catalysts. Inset in (a) is the SAED pattern of the Ni–B particles. Reproduced from ref. 154 with kind permission from Elsevier.

Using the reductant-impregnation strategy, Chen *et al.* prepared SBA-15-, MCM-41-, and HMS-supported Ni–B catalysts.[153,154] The Ni–B nanoparticles were uniformly dispersed in the SBA-15 channels, with the average particle size of *ca.* 6 nm. While on MCM-41 or HMS with a channel size of *ca.* 3 nm, the Ni–B nanoparticles were mainly located on the external surface bearing much larger particle size (Fig. 7). Similarly, nearly all Co–B nanoparticles were confined in the channels of SBA-15, while most Co–B nanoparticles agglomerated on the exterior of MCM-41.[155] Moreover, for commercial SiO_2-supported Ni–B and Co–B catalysts, the Ni–B[154] and Co–B particles[155] were predominantly situated on the exterior, although the average pore diameter of commercial SiO_2 was much larger than those of MCM-41 and HMS and slightly larger than that of SBA-15. It seems that the regular and large mesopores and the micropores connecting the mesopores are essential for the retainment of amorphous alloy nanoparticles in the channels of SBA-15, since its pseudo-3D pore structure can facilitate the rapid dissipation of the released H_2, which otherwise expels the nanoparticles out of the channels.

Grafting of functional groups on the channel walls of regular mesoporous silicas induced the deposition of the Ni–B nanoparticles on the interior surface.[156] For conventional Ni–B/SBA-15 prepared by $NiCl_2$ impregnation followed by KBH_4 reduction, most of the Ni–B nanoparticles were located on the external surface. When SBA-15 was grafted with the aminopropyl (NH_2) groups, the same preparation method led to homogeneous distribution of Ni–B nanoparticles in the mesoporous channels, attributable to the coordination of the Ni^{2+} ions with the grafted NH_2 groups. The smooth reduction of the NH_2-coordinated Ni^{2+} ions can effectively suppress the drastic release of H_2. The grafting of CH_3 groups on the channel walls of SBA-15 also improved the

distribution of the Ni–B nanoparticles,[156] which is explained by the enhanced surface hydrophobicity that slowed down the reaction between Ni^{2+} ions and BH_4^-.[157] Surface grafting also increased the surface B content for Ni–B supported on NH_2–SBA-15 and CH_3–SBA-15, with a more prominent increment observed on the former.

Besides regular mesoporous silicas, carbon nanotubes (CNTs) with uniform mesopores are suitable as a support for encapsulating amorphous alloy nanoparticles. Wang *et al.* synthesized the Ni–B/CNTs catalyst by $NiCl_2$ impregnation followed by KBH_4 reduction.[158] As compared to Ni–B/γ-Al_2O_3, the Ni–B nanoparticles on CNTs are more dispersed. The thermal stability of Ni–B/CNTs is better than Ni–B/γ-Al_2O_3, since the unique pore structure of the CNTs protects Ni–B nanoparticles from aggregation. Furthermore, CNTs may donate electron to Ni, leading to active sites enriched with more electrons.

5. Catalytic applications

Because of their attractive structural and electronic characters, the chemically reduced metal–metalloid amorphous alloys have been employed to catalyze a wide range of reactions. The reactions involved are extended from model reactions to industrially more relevant reactions, from non-selective reactions to more challenging selective hydrogenation, hydrogenolysis, dehydroheteroatom, energy/fuel production, pollutant removal, and bond forming reactions, as will be described in the following context.

5.1 Hydrogenation of olefinic bonds

5.1.1 Hydrogenation of acrylonitrile. Hydrogenation of acrylonitrile to propionitrile is an important process for industrial synthesis of dichloropropionate used in herbicides. For this reaction, the Ni–B/SiO_2 amorphous alloy catalyst showed higher intrinsic activity than the Ni/SiO_2 catalyst.[159] The calcination temperature before and after chemical reduction of the catalyst affected the activity.[160] For the catalyst precursor, the optimal calcination temperature is 473 K. Calcination of the as-reduced catalyst up to 573 K did not deteriorate the activity. Microwave heating of the catalyst precursor led to Ni–B/SiO_2 with a hydrogen uptake rate of 0.117 mmol s^{-1} g_{Ni}^{-1}, as compared to 0.068 mmol s^{-1} g_{Ni}^{-1} on the catalyst without microwave heating.[134] However, microwave heating did not change the intrinsic activity.

5.1.2 Hydrogenation of tricyclopentadiene (TCPD). The hydrogenation of TCPD through dihydrotricyclopentadiene (DHTCPD) to tetrahydrotricyclopentadiene (THTCPD) is of great importance (Scheme 4),[161] as THTCPD provides more propulsive energy than traditional fuels from refinery.[162] In general, the second hydrogenation step is kinetically more difficult than the first one.[163] Zhang and coworkers reported that the Pd–B/γ-Al_2O_3 catalyst exhibited higher activity for the successive hydrogenation of DHTCPD than Pd/γ-Al_2O_3 reduced by H_2, with the selectivity of 76% to the production of THTCPD on the former and 68% on the latter at similar conversion levels of TCPD.[161] The better catalytic performance of the amorphous alloy catalyst was attributed to its higher H_2 adsorption capacity, since the hydrogenation activity depended linearly on the amount of H_2 adsorbed.[164]

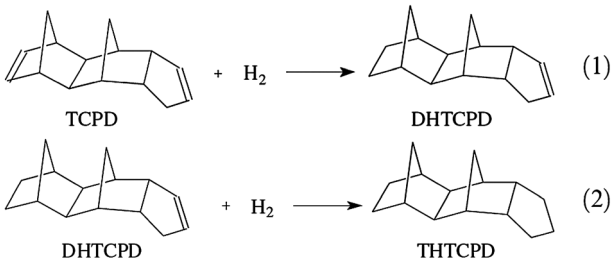

Scheme 4 Hydrogenation of TCPD to THTCPD. Reproduced from ref. 161 with kind permission from Elsevier.

5.1.3 Hydrogenation of sulfolene. Hydrogenation of sulfolene to sulfolane is an important industrial process due to the wide application of sulfolane as a solvent for both extraction and reaction.[165] Mostly, the hydrogenation is carried out in the liquid phase at elevated hydrogen pressure over RANEY® Ni. However, the serious disadvantage of RANEY® Ni such as short lifetime due to sulfur poisoning makes it necessary to develop catalysts with excellent activities.

Tao and coworkers investigated the catalytic performance of Ni-based amorphous alloy catalysts in sulfolene hydrogenation. The Ni–Co–B amorphous alloy catalyst with a Ni/Co molar ratio of 2.3 exhibited a sulfolane yield of 98%, higher than the yield of 86% on RANEY® Ni under the same reaction conditions.[166] The Ni–P amorphous alloy catalysts prepared at 283–303 K had high specific surface area (200–300 m^2 g^{-1}), thus high catalytic activity.[167] The supports for the Ni–B amorphous alloy catalysts played an important role in the activity. With the same catalyst weight, the TiO_2-supported Ni–B catalyst with a Ni loading of 7.20 wt% exhibited comparable sulfolane yield to that of the unsupported Ni–B.[168] The MgO-supported Ni–B catalyst exhibited remarkably higher activity than Ni–B/TiO_2.[143,144] The superior activity of Ni–B/MgO was attributed to the promotion effects of MgO on the characteristics of the Ni–B particles, the distribution of Ni–B particles, as well as the active surface area of Ni. Moreover, the initial catalytic activity of Ni–B/expanded graphite was about twice of that Ni–B/MgO.[169] Using chitosan-mediated expanded graphite as a support could further improve the catalytic activity.[170]

5.2 Hydrogenation of the phenyl ring

5.2.1 Complete hydrogenation of benzene. Hydrogenation of benzene to cyclohexane is a basic reaction in the petrochemical industry and environment protection. Cyclohexane is the precursor for the manufacture of nylon-6 and nylon-66. Since benzene hydrogenation was realized for the first time using finely divided Ni as a catalyst by Sabatier in 1926,[171] this reaction has been extensively studied.[172] Up to now, the hydrogenation of benzene to cyclohexane is still an active area of research.[173,174]

Deng and coworkers found that under the same reaction conditions, the Ni–B/γ-Al_2O_3 catalyst prepared by the two-step drying approach gave a benzene conversion of 95%, as compared to 69% on the catalyst prepared by the conventional method.[64,175]

While both catalysts displayed identical turnover frequencies (TOFs), the higher benzene conversion on the former was due to the improved dispersion of the active sites by the modified drying approach. Zhang *et al.* employed bentonite and CNTs as supports for Ni–B for gas phase hydrogenation of benzene.[176] They identified that the Ni–B/bentonite catalyst was more active and more resistant to sulfur poisoning than Ni/bentonite. Ni–B/bentonite also showed better catalytic performance than Ni–B/Al_2O_3, owing to the better dispersion of Ni–B and the stronger acidity of bentonite. On Ni–B/CNTs, the benzene conversion was 58% at 363 K, while a similar conversion was obtained at 20 K-higher on Ni–B/γ-Al_2O_3, which was attributed to the unique electronic property and pore structure of the CNTs.[158,177] High benzene conversion was reported on the Ru–B/CNTs catalyst with a low Ru loading of less than 0.5 wt%.[178]

The Ni–P catalysts exhibited higher TOFs than RANEY® Ni in benzene hydrogenation.[179] However, they are far less active than Ni–B.[180] In addition, no significant S resistance was observed on Ni–P.[22] On the other hand, the superior thermal stability of Ni–P[180] implies that it may be more suitable for high-temperature reactions. The thermal stability of Ni–P was further improved by supporting on CNTs.[181] And the weight specific activity of Ni–P/CNTs was *ca.* four times of the unsupported Ni–P nanoparticles.

Co,[22,34,78] W,[77,179] rare earth metals (La, Sm, Yb, Nd),[176,182] and Pt[183] are effective promoters for amorphous alloy catalysts in benzene hydrogenation. The promotion effect of Co on Ni–B was the most prominent at the Co/Ni molar ratio of unity. The areal specific activity of the optimal Ni–Co–B catalyst is *ca.* five times of that of Ni–B.[34] By further incorporating W into Ni–Co–B, the TOF was doubled, and after as much as 30 times of reuse the catalytic activity was dropped to one half of the original value, likely due to the presence of residual oxygen in the reaction system.[77] Similarly, Li and Xu found that promotion of Ni–P/SiO_2 by W increased the intrinsic activity.[179] La, Sm, Yb, and Nd not only enhanced the catalytic activity, but also improved S resistance.[176,182] Addition of a small quantity of Pt (0.07 wt%) to Ni–B/*pseudo*-boehmite-modified mordenite drastically improved the catalytic activity and S resistance.[183] The reaction temperature required for complete conversion of benzene was reduced by 50 K in the presence of Pt.

5.2.2 Partial hydrogenation of benzene. Hydrogenation of benzene to cyclohexene is of great industrial interest, since cyclohexene can be easily converted to value-added cyclohexanol, caprolactam, and adipic acid by typical olefin reactions. However, to obtain cyclohexene from benzene is thermodynamically less favorable (Scheme 5). In 1999, Xie *et al.* reported that the Ru–B/SiO_2 catalyst exhibited excellent selectivity to cyclohexene,[184] which aroused extensive research interest in partial hydrogenation of benzene over amorphous alloy catalysts.

The effect of the content elemental B in Ru–B on the selectivity to cyclohexene was investigated in the literature.[28] The cyclohexene selectivity increased remarkably from 25% to 51% when the B content increased from 1.9 to 10.1 mol%, which are higher than the value of 19% on Ru powder reduced by H_2.

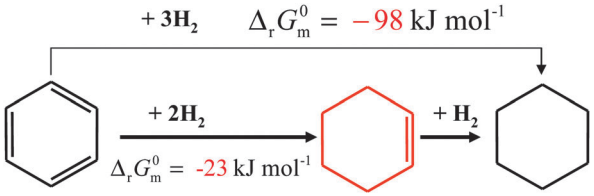

Scheme 5 Hydrogenation pathway of benzene to cyclohexene and cyclohexane.

The size of the Ru–B nanoparticles is another important factor influencing the selectivity to cyclohexene. On PVP-stabilized Ru–B colloids in the size range of 1.3 to 3.9 nm, Bu *et al.* identified that smaller particle size led to higher activity and higher cyclohexene selectivity.[93] The cyclohexene yield of *ca.* 17% was obtained on the 1.3 nm-PVP-Ru–B colloids in the absence of any additional reaction modifier.

On the Ru–B/SiO_2 catalyst the cyclohexene selectivity was 50%, which was much higher than 22% on Ru/SiO_2 reduced by H_2.[184] To achieve a high cyclohexene selectivity, the hydrophilicity of the support plays an important role.[185–187] Wang *et al.* reported that the Ru–B/Al_2O_3·$x$$H_2O$ colloidal catalyst is more active and selective than Ru–B/γ-Al_2O_3.[188] Activity and selectivity enhancement was also observed on a Ru–B colloidal catalyst stabilized by *in situ* formed silica as compared to commercial SiO_2-supported catalysts.[189]

Liu *et al.* investigated the effect of the preparation method and the types of zirconia on the catalytic performance of Ru–B.[190] The Ru–B/ZrO_2·$x$$H_2O$ catalyst prepared by the chemical mixing method, similar to the sol–gel method, exhibited an impressive cyclohexene selectivity of 50% in the absence of reaction modifiers, as compared to 20% and 15% on Ru–B/ZrO_2·$x$$H_2O$ and Ru–B/ZrO_2 prepared by the conventional method, respectively, and 28% on the unsupported Ru–B. On the Ru/ZnO–$ZrO_x(OH)_y$ catalyst prepared by the chemical mixing method and reduced by $NaBH_4$, a cyclohexene selectivity of 72% was reported at a benzene conversion of 78% without the aid of reaction modifiers.[191]

The promoters can enhance the cyclohexene selectivity on Ru–B by stabilizing the hydrogenation intermediate,[190] by improving the dispersion of the active sites,[192] or by promoting the formation of electron-deficient active species.[193] It is found that the addition of 2.5 wt% of Zn to Ru–B/ZrO_2·$x$$H_2O$ increased the cyclohexene yield from 33% to 46% without the aid of reaction modifiers.[190] The same promotion effect of Zn was observed on Ru/ZnO–$ZrO_x(OH)_y$, on which the cyclohexene yield amounted to 56% at the Zn/Zr molar ratio of 10, while it was only 6.8% on Ru/$ZrO_x(OH)_y$.[191] La,[192] Co,[193] and Fe[194,195] also showed a positive effect in partial hydrogenation of benzene. Addition of La to Ru–B/ZrO_2 increased the activity and selectivity.[192] On Ru–Co–B/γ-Al_2O_3, the maximum yield of cyclohexene was 29% with a cyclohexene selectivity of 46% in the absence of reaction modifiers.[193] On Ru–Fe–B/ZrO_2, a cyclohexene yield of 57% at a benzene conversion of 81% was reported.[195]

5.3 Hydrogenation of carbonyl groups

5.3.1 Hydrogenation of glucose. Sorbitol is widely used as a starting feedstock for Vitamin C synthesis, an emulsifier for fatty acid ester production, an intermediate for drug design,

and an additive in food, cosmetic and paper products. Although there is natural sorbitol, its large-scale production always depends on the catalytic hydrogenation of glucose most frequently on RANEY® Ni.[196] Ni–B nanoparticles were found to be about one order of magnitude more active than RANEY® Ni in glucose hydrogenation.[197] Promotion of Ni–B by W further enhanced the catalytic activity. The apparent activation energy on the nanosized Ni–W–B was 54.7 kJ mol^{-1}, lower than 81.5 kJ mol^{-1} determined on RANEY® Ni. Chemical reduction of nickel ions complexed with ethylenediamine or hydrazine under ultrasonication led to Ni–B catalysts more active than conventional Ni–B and RANEY® Ni.[198,199]

Ru–B was highly active in glucose hydrogenation, showing intrinsic activity about 11–20 times of that of Ni–B or Co–B.[58] The superior activity of Ru–B can be related to its especially low apparent activation energy of 14.5 kJ mol^{-1}. Ru–B can be used repetitively for more than 13 times without significant deactivation, showing its excellent durability. Promotion of Ru–B with Cr decreased the intrinsic activity, but the catalyst showed higher weight specific activity due to the improved surface area.[200] Supporting Ru–B on SiO_2 further increased the intrinsic activity.[201]

5.3.2 Hydrogenation of fructose. Mannitol is extensively used in food and pharmaceutical industries as a non-toxic, non-hygroscopic, and low caloric sweetener. In industry, mannitol is produced by catalytic hydrogenation of fructose or syrups (mixtures of glucose and fructose), with sorbitol as the main byproduct (Scheme 6). Hydrogenation of pure fructose over conventional Ni-based catalysts gave mannitol selectivity and yield of *ca.* 45–50%.[202] The industrial hydrogenation of invert sugar (glucose/fructose = 1/1, obtained by the hydrolysis of sucrose) over RANEY® Ni produced a mixture of mannitol and sorbitol in a weight ratio of about 25/75.[203] Liaw and coworkers found that Co–Ni–B and PVP-stabilized Co–Ni–B are much more active than Ni–B, Co–B, and RANEY® Ni in the hydrogenation of fructose and invert sugar.[85] Moreover, PVP-Co–Ni–B is about twice as active as Co–Ni–B in fructose hydrogenation. Although the selectivity to mannitol was improved only slightly to above 30% in the hydrogenation of invert sugar, the highly active Co–Ni–B and PVP–Co–Ni–B are promising to replace RANEY® Ni for this reaction.

5.3.3 Hydrogenation of maltose. Hydrogenation of maltose to maltitol is important owing to the applications of maltitol

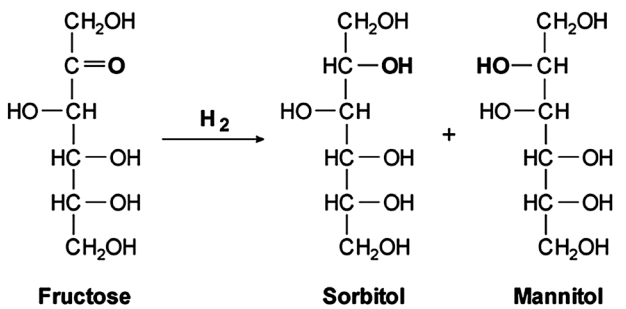

Scheme 6 Hydrogenation of fructose.

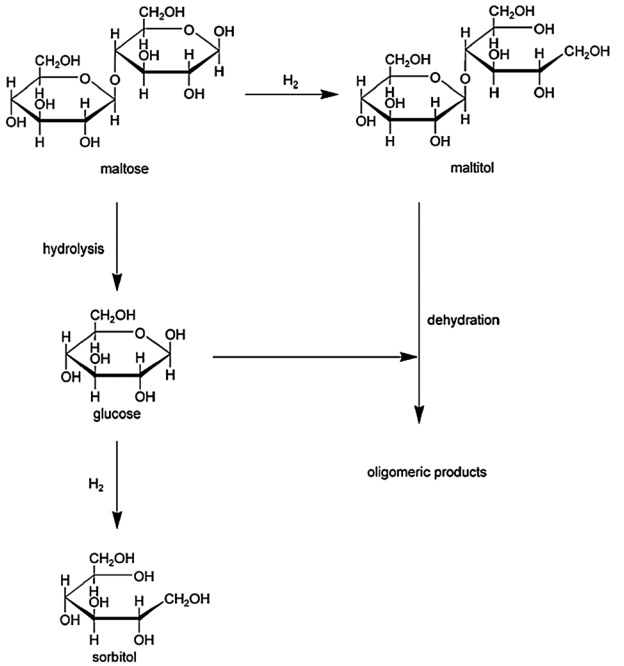

Scheme 7 Reaction network for maltose hydrogenation. Reproduced from ref. 206 with kind permission from Wiley-VCH.

as a sugar substitute in modern nutrition and in diabetic food, and as an intermediate for pharmaceutical production.[204] Although RANEY® Ni is widely used in this industrial process, the leaching of Ni during hydrogenation and the poor selectivity to maltitol make this catalyst less profitable.[205] Amorphous alloy catalysts are excellent for this reaction. Ni–P, Ru–P,[206] Ru–B,[98,121,206] Co–P,[206,207] Co–B, and Co–P–B[207] displayed maltitol selectivity up to 100%. For comparison, only 75% selectivity was obtained on RANEY® Ni due to the formation of sorbitol and trace amounts of undefined byproduct (Scheme 7).[206] Moreover, the amorphous alloy catalysts exhibited higher intrinsic activity than RANEY® Ni.[206] These merits signify that amorphous alloy catalysts are attractive alternatives to RANEY® Ni in the hydrogenation of maltose to maltitol.

As compared to Co- and Ni-based amorphous alloy catalysts, Ru-based amorphous alloy catalysts showed much higher activity in the hydrogenation of maltose.[206] The intrinsic activity was ranked as Ru–P > Ru–B ≫ Co–P > Ni–P ≫ RANEY® Ni. Ru–P also exhibited a weight specific activity nearly one order of magnitude of that of Ru–B, despite the higher dispersion degree of Ru–B. The apparent activation energy of maltose hydrogenation is 27 kJ mol^{-1} and 32 kJ mol^{-1} on Ru–P and Ru–B, respectively. In addition, Ru–P and Ru–B are more durable than RANEY® Ni in the recycling test, since they are more vulnerable to leaching.

Because Ru is expensive,[208] it is desirable to enhance its utility by synthesizing catalysts with large active surface area. On worm-like mesoporous Ru–B with an active surface area of 33.8 $m^2 g^{-1}$, the weight specific activity was drastically increased to 662 mmol h^{-1} g^{-1}, as compared to 176 mmol h^{-1} g^{-1} on conventional Ru–B.[121] The monodispersed Ru–B nanoparticles with an average size of 2.4 nm are nearly two times more active than conventional Ru–B.[98] The intrinsic activity of the former

was also enhanced, suggesting that reduction of the catalyst under ultrasound additionally modified the nature of the active sites.

Since the intrinsic activity of Co–P is more than three times of that of Co–B, its active surface area is about one third of that of the latter, to take full advantages of the promotion effects of both P and B, ternary Co–P–B was prepared for maltose hydrogenation.[209] On $Co_{72.2}P_{5.9}B_{21.9}$, the weight specific activity is 2.6 times of that of Co–P, and more than three times of that of Co–B. Although the weight specific activity of $Co_{72.2}P_{5.9}B_{21.9}$ is about one half of that of Ru–B,[206] considering that Ru is about two orders of magnitude more expensive than Co, the ternary Co–P–B is a cost-effective candidate for the hydrogenation of maltose to maltitol.

5.3.4 Chemoselective hydrogenation of unsaturated aldehydes and ketones. Chemoselective hydrogenation of unsaturated aldehydes or ketones results in unsaturated alcohols that are valuable and versatile intermediates in the synthesis of fine chemicals, pharmaceuticals, flavors, fragrances, and herbicides.[210] This reaction is also of great scientific importance, because the saturated aldehydes or ketones are thermodynamically more favorable. Selectivity manipulation is generally achieved by activating the carbonyl group and/or suppressing the adsorption of the conjugated olefinic bond or the phenyl ring.[211]

Ni-,[81,82,86,128] Co-,[41,80,90,96,124,212–214] and Ru-based amorphous alloy catalysts[95,215,216] have been investigated in chemoselective hydrogenation of unsaturated aldehydes or ketones. In the hydrogenation of furfural (FFR) to furfuryl alcohol (FFA), Mo, Ce, and Fe are effective promoters for Ni–B or Co–B. As compared to Ni–B/γ-Al_2O_3, Ni–Mo–B/γ-Al_2O_3 drastically improved the FFR conversion from 19% to 91% and the FFA selectivity from 87% to 95%.[82] The weight specific activity of Ni–Ce–B is *ca.* 2.8 times of that of Ni–B, and FFA was formed almost exclusively.[81] Fe is more effective than Ce in enhancing the activity and selectivity of Ni–B.[86] On the other hand, although the weight specific activity of Co–B is much lower than that of Ni–B, promotion by Mo drastically enhanced the activity of Co–B by 4.7 times, and Co–Mo–B exhibited up to 100% FFA selectivity.[80] In the hydrogenation of crotonaldehyde (CRAL) to crotyl alcohol (CROL) (Scheme 8), Pei *et al.* investigated the promotion effects of Sn,[212] Zn,[213] and Fe on Co–B.[41,214] Among these promoters, Fe showed the best promotion effect, giving rise to the CROL yield of 63%, higher than those obtained on Pt-based catalysts.[41,214] The Sn-promoted Ru–B/SiO_2 catalyst is highly active and selective in the hydrogenation of carbonyl compounds to the corresponding alcohols at low temperature.[215]

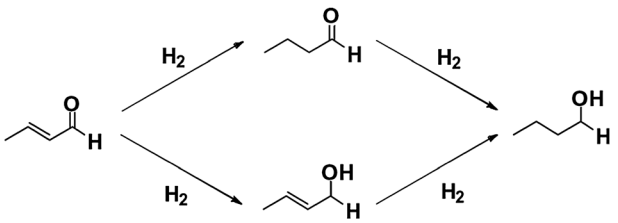

Scheme 8 Reaction pathways of CRAL hydrogenation.

At 333 K, the benzaldehyde conversion over Ru–Sn–B/SiO_2 is nearly five times of that over Ru–B/SiO_2. The hydrogenation of cinnamaldehyde (CMA), phenylacetaldehyde, aliphatic carbonyl compounds (capryl aldehyde and methyl hexyl ketone), diphenylketone, pyridine-2-carboxaldehyde, and 4-methoxybenzaldehyde was also evaluated at 333 K on Ru–Sn–B/SiO_2, giving appreciable conversion and exclusive selectivity to alcohols, although the last two compounds are less reactive than others.

Morphology control is another effective means to improve the catalytic performance of the amorphous alloy catalysts. A hexagonal Ni–B nanoarray is more active and selective than conventional Ni–B in the hydrogenation of acetophenone to 1-phenylethanol.[128] Uniform spherical Co–B nanoparticles gave rise to the cinnamyl alcohol (CMO) selectivity of 99% at a CMA conversion of 92%, which is far more selective than RANEY® Co.[96] The catalytic performance was further enhanced on Co–B nanoparticles synthesized in the O/W microemulsion.[90] On mesoporous Co–B, the CMO selectivity is 94% at a CMA conversion of 97%, which is *ca.* 10% higher than that over conventional Co–B.[124]

5.3.5 Chemoselective hydrogenation of 2-ethylanthraquinone (eAQ). The hydrogenation of eAQ to 2-ethylanthrahydroquinone (H_2eAQ) is a key step in industrial manufacture of H_2O_2, a green oxidizing agent (Scheme 9).[217] However, even on the most selective Pd catalyst, during the hydrogenation eAQ will be deeply hydrogenated to some degradation products that cannot be oxidized to produce H_2O_2, leading to the loss of the expensive eAQ and fed H_2. Besides, the oxidation rate of H_4eAQH_2 is remarkably lower than that of eAQH_2, thus leading to lower production efficiency.[83]

Promoted and supported Ni–B catalysts are highly effective in chemoselective hydrogenation of eAQ. Nanosized Ni–Cr–B is more active than RANEY® Ni, and displayed 100% selectivity to eAQH_2 at complete conversion of eAQ.[83,218] Nanosized Ni–La–B[219] and Ni–Mo–B[220] showed a H_2O_2 productivity of $\sim$7.5 and 6.9 $mg_{H_2O_2}\ g_{cat}^{-1}\ min^{-1}$, respectively, which are much higher than the productivity of 3.7 $mg_{H_2O_2}\ g_{cat}^{-1}\ min^{-1}$ on RANEY® Ni.

Chen *et al.* studied the effect of supports on the catalytic properties of Ni–B.[221] The catalytic activity is in the order of Ni–B/SiO_2 > Ni–B/Al_2O_3 > Ni–B/AC, and the selectivity to carbonyl group hydrogenation is in the order of

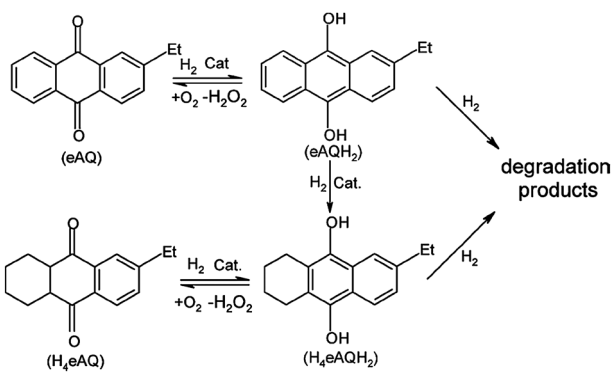

Scheme 9 The hydrogenation and oxidation cycles of eAQ and H_4eAQ. Reproduced from ref. 217 with kind permission from Elsevier.

Ni–B/AC > Ni–B/SiO_2 > Ni–B/Al_2O_3 > RANEY® Ni. HMS-, MCM-41-, and SBA-15-supported Ni–B exhibited higher selectivity than the commercial SiO_2-supported one.[153,154] Although on all these supported Ni–B catalysts the maximum H_2O_2 yield of ~100% was obtained, the yield of H_4eAQH_2, the phenyl ring hydrogenation product, follows the sequence of Ni–B/SiO_2 > Ni–B/MCM-41 > Ni–B/HMS > Ni–B/SBA-15. It is notable that on Ni–B/SBA-15, eAQH_2 is the only product at the maximum yield of H_2O_2.

5.4 Amine production

5.4.1 Hydrogenation of nitro compounds. Amines have wide industrial applications in manufacturing engineering plastics, water treatment chemicals, surfactants, agrochemicals, and pharmaceuticals. Catalytic hydrogenation of nitro compounds is an important route for the production of amines. In the hydrogenation of 4,4′-dinitro-diphenylether to 4,4′-amino-diphenylether, the TOF over the Ni–B/AC catalyst prepared by the reductant impregnation method is 0.332 s^{-1}, about three times of that over the catalyst prepared in the conventional impregnation sequence.[139] In the hydrogenation of *p*-nitrophenol to *p*-aminophenol (PAP), Pd–B/TiO_2 exhibited higher activity, selectivity, and stability than other Pd-based and Ni-based catalysts.[222] The catalytic activity sequence is Pd–B/TiO_2(2%) ≈ Pd–B/TiO_2(0.5%) ≈ Pd/C(2%) > Pd/TiO_2 ≈ nano-sized Ni > Pd–B > RANEY® Ni. PAP is the only product on all catalysts, with the exception of RANEY® Ni.

Catalytic transfer hydrogenation represents an important form of catalytic hydrogenation using hydrogen donor reagents such as hydrazine hydrate, formic acid or isopropyl alcohol as a substitution for H_2. The catalysts involved in catalytic transfer hydrogenation include Pt, Pd, Ru, and Ni in the form of complexes.[223,224] Wen *et al*. employed polymer-supported Ni–B in catalytic transfer hydrogenation of aromatic nitro compounds with hydrazine hydrate.[225] Single nitro group compounds were reduced smoothly and gave excellent yields up to 100%. For dinitro compounds, only one nitro group was reduced, and gave moderate yields (≥ 70%). The catalyst is stable and reusable. The attractive catalytic performance of the Ni–B/polymer catalyst is explained by the unique electronic character of Ni–B and its high activity in decomposing hydrazine hydrate.

5.4.2 Hydrogenation of nitriles. Hydrogenation of nitriles is another important route for amine production, in particular primary amines.[226] Ethylamine (EA) is an intermediate widely used in medicine and surfactant production, as well as in organic synthesis. Hydrogenation of acetonitrile (AN) is a promising route for ethylamine production, however, the selectivity is a critical issue. Except for primary amine, the secondary and even the tertiary amines may form.[227] Moreover, condensed byproducts may occur by transamination reactions between amines and imines (Scheme 10).[228] RANEY® Ni, Co, and noble metals are common catalysts for the hydrogenation of nitriles. The selectivity to ethylamine is low on RANEY® Ni and Co-based catalysts,[229] while high cost and poor S and N resistance are involved for noble metal catalysts.[230]

A comprehensive investigation of the hydrogenation of AN to EA on Co- and Ni-based amorphous alloy catalysts has been undertaken by Li and coworkers.[50,230–232] Ni–B exhibited higher activity and selectivity to EA than ultrafine Ni powder, RANEY® Ni, and crystallized Ni–B. The EA yield over Ni–B reached 68%, much higher than that over RANEY® Ni (<40%).[230] Similarly, Co–B exhibited much higher activity and selectivity to EA than RANEY® Co, pure Co powder, and crystallized Co–B.[50] Co–B is also superior to Ni–B in terms of selectivity and yield of EA, and lifetime. Remarkably, the intrinsic activity of Ni–Co–B is nearly twice of that of Ni–B or Co–B at the Co/Ni molar ratio of 1.[232] The EA selectivity leveled off at this Co/Ni ratio, leading to a maximum EA yield of 93%.

Selective hydrogenation of unsaturated nitriles to unsaturated amines is of considerable challenge, since the hydrogenation of the olefinic bond is thermodynamically more favorable than the nitrile group. Molecules with olefinic and nitrile groups in conjugation or in close proximity are even more difficult to reduce selectively.[233,234] Kukula *et al*. reported that Ni–B and Cr-promoted Ni–B favor the hydrogenation of the olefinic bond, whereas Co–B and Cr-promoted

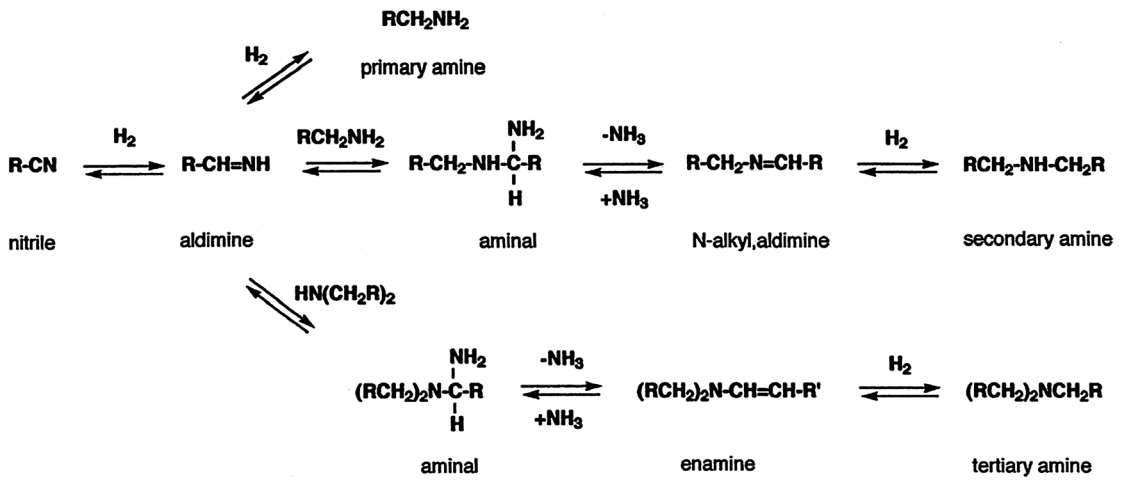

Scheme 10 Formal reaction scheme for nitrile hydrogenation. Reproduced from ref. 228 with kind permission from Elsevier.

Co–B favor the formation of the unsaturated amine.[235] The Cr-promoted Co–B treated with NaOH hydrogenated cinnamonitrile, 1-cyclohexenyl-acetonitrile, and *trans*-3-pentenenitrile to the corresponding primary unsaturated amines with medium-to-high selectivities without the aid of ammonia at high conversion levels.

5.5 Hydrodeheteroatom

5.5.1 Hydrodesulfurization (HDS). Catalytic HDS is a key process in oil refinery to upgrade the oil and to remove environmental pollutants. Typically, metal sulfide catalysts are used, but the activity and lifetime are limited.[236] Tao and coworkers investigated the kinetics of Ni–B/TiO_2 and Ni–B/Al_2O_3 in HDS of thiophene.[237] Ni–B/TiO_2 is more active than Ni–B/Al_2O_3, since the apparent activation energy on the former is only 43.5 kJ mol^{-1}. Bussell and coworkers identified that catalysts prepared by sulfiding Ni–B/SiO_2 and Ni–Mo–O–B/SiO_2 showed significantly higher thiophene HDS activities than conventional sulfided Ni/SiO_2 and Ni–Mo/SiO_2 catalysts.[238] The activity of sulfided Ni–Mo/SiO_2 decreased more rapidly such that its activity is 70% of that of the sulfided Ni–Mo–O–B/SiO_2 after 24 h on stream, which is traced to the higher density of active sites on the amorphous alloy catalysts. It is notable that crystalline Co_2B and Ni_3B have relatively low activities and are unstable under HDS conditions.[239] Addition of Mo to Ni–B/boehmite drastically increased the conversion of thiophene from 43% to 74% at a low HDS temperature of 493 K.[240]

5.5.2 Hydrodechlorination (HDC). The HDC of the carcinogenic and mutagenic aromatic chlorides can convert chlorinated waste into products of commercial value.[241] Partially crystallized Ni–P/SiO_2 exhibited initial weight specific activity *ca.* 67% higher than Ni/SiO_2 in the HDC of chlorobenzene (CB).[242] Pd/Ni–B/TiO_2 prepared by replacement of Ni–B nanoparticles with Pd^{2+} ions and treated in N_2 at 473 K exhibited better activity and stability than Pd/PVP, a mixture of Pd and Ni–B nanoparticles, and Pd/Ni obtained by the replacement of nanocrystalline Ni with Pd^{2+} ions.[243] After the 4th recycle, the CB conversion on Pd/Ni–B/TiO_2 is still comparable to that on the Pd/Ni catalyst of the first run.

5.5.3 Hydrodeoxygenation (HDO). The conversion of lignin or wood biomass to bio-oil is a promising alternative for solving the problem of rapid decline of crude oil resources. However, oxygen-containing compounds like phenol and cyclopentanone in bio-oil lead to deleterious properties such as corrosion, high viscosity, poor heat value, thermal instability, immiscibility with hydrocarbon fuels, and tendency of polymerization during storage and transportation.[244] It is necessary to remove these oxygen-containing compounds to expand the utilization of bio-oil. Among technologies for bio-oil upgrading like HDO and catalytic cracking, the former has attracted much attention owing to the high yield of hydrocarbons and low yields of tar and coke.[245] Yang and coworkers investigated the catalytic properties of Ni–Mo–B, Ni–W–B, and Co–Mo–B catalysts for the HDO of phenol.[246] The Ni–Mo–B prepared by ultrasound-assisted reduction exhibited higher activity than the conventional amorphous alloy catalyst. On Ni–Mo–B, the selectivity to oxygen-free products is 93% (including 12% of benzene) at a phenol conversion of 81%. The addition of Co or La to conventional Ni–Mo–B drastically increased the selectivity to deoxygenation products from 27% to 93% with a low benzene selectivity of 3.2% on Co–Ni–Mo–B.[247,248] The total H/C atomic ratio in the products was increased from 1.95 on Ni–Mo–B to 1.99 on La–Ni–Mo–B. The addition of Co and La to Ni–W–B improved the selectivity of deoxygenation products to 86%[249] and 68%,[250] respectively, while benzene was not formed, which is desirable for clean fuel production. Co–Mo–B exhibited high catalytic activity in the HDO of phenol, benzaldehyde, and acetophenone; both the conversion and the deoxygenation selectivity approached 100%, with low selectivity to benzene.[251,252] For the HDO of cyclopentanone, Co–W–B exhibited a low cyclopentanol selectivity of 0.4% and a high deoxygenation selectivity of 95% at a cyclopentanone conversion of 97%,[253] showing that the amorphous alloy catalyst is a potential candidate for the HDO process.

5.6 Fischer–Tropsch synthesis (FTS)

FTS is essential for the transformation of coal and biomass to clean transportation fuels and value-added chemicals. The active metals for FTS are Ru, Fe, Co, and Ni. Ni is usually not used in FTS due to its high CH_4 selectivity.[254] Amorphous alloy nanoparticles may exhibit excellent FTS performance under mild reaction conditions due to their high surface area, small particle size, and high population of CUSs, which are advantageous to adsorption and surface reactions. These merits offer the opportunity to the development of energy-efficient and cost-effective Fe- and Co-based amorphous alloy catalysts active in low-temperature FTS reaction. Conventional Fe- and Co-based FTS catalysts are active only above 473 K.[255]

5.6.1 FTS on Ni-based catalysts. Nanosized Ni–B, Ni–P, and Ni–P–B were used for gas phase FTS at 573 K, 0.1 MPa, $H_2/CO = 2$, and $F/W = 5400$ ml h^{-1}.[256] Attractively, the selectivities to C_2–C_4 hydrocarbons are as high as 89% on $Ni_{83}P_{17}$ and 68% on $Ni_{67}B_{33}$, which are higher than the value expected by the Anderson–Schulz–Flory (ASF) distribution law (C_2–C_5 < 55%).[21] In sharp contrast, crystallized $Ni_{67}B_{33}$ was only selective to CH_4, signifying the importance of the amorphous structure in the FTS selectivity.

5.6.2 FTS on Ru–B. Kou and coworkers used the PVP-stabilized Ru–B nanocatalyst to catalyze the FTS reaction in aqueous phase.[257] This catalyst showed a superior weight specific activity of 1.6 mol_{CO} mol_{Ru}^{-1} h^{-1} to Ru/SiO_2 and Ru/C catalysts at 423 K, 2.0 MPa of H_2, and 1.0 MPa of CO. It is noteworthy that since the hydrocarbon products are immiscible with water, they can be easily separated from the solvent and the catalyst, which simplifies the working up process and improves the production efficiency.[258]

5.6.3 FTS on Co–B. The FTS performance of the Co–B nanocatalyst has been studied in aqueous phase (stabilized by PVP) or PEG200 under mild reaction conditions (403–443 K, 2.0 MPa of H_2, and 1.0 MPa of CO).[259] Co–B nanoclusters with a size of ~5 nm are active at low temperature with weight

specific activities of 0.03–0.12 mol_{CO} mol_{Co}^{-1} h^{-1}. When the reaction was carried out in ethylene glycol (EG), syngas was converted not only to hydrocarbons, but also to 2-alkyl-dioxolanes with the participance of EG.[260] In this case, the Co–B nanocatalyst exhibited an activity of 0.07 mol_{CO} mol_{Co}^{-1} h^{-1}, and selectivities to dioxolanes of 31 wt% and hydrocarbons of 69 wt%. Wang *et al.* prepared two Co–B/faujasite catalysts, with one with Co–B particles of *ca.* 1–2 nm probably located in the supercages of faujasite, and the other with particle size >10 nm mainly outside of the cages.[261] In gas phase FTS reaction, Co–B/faujasite with smaller particle size showed remarkably higher CO conversion, higher selectivity to C_5–C_{21} hydrocarbons, and lower selectivity to C_{21+} hydrocarbons than that with larger nanoparticles.

5.6.4 FTS on Fe–B. Nanosized Fe–B with various Fe/B ratios were prepared by Zong *et al.* for gas phase FTS reaction.[256] Although these catalysts are far less active than Ni-based amorphous alloy catalysts mentioned above, the main products on Fe–B are highly desirable C_2–C_3 olefins, and the selectivity increased with the B content. The selectivity to C_2–C_3 olefins amounted to 74% on $Fe_{60}B_{40}$, which is substantially higher than the value predicted by the ASF distribution.

There are a number of works focusing on using Fe–B nanoparticles in liquid phase FTS reaction at low temperatures (≤473 K). Wu and coworkers prepared the Fe–B nanocatalyst with the size of 30–65 nm and evaluated its FTS performance in PEG400 at 473 K.[262] This catalyst exhibited excellent activity and stability, as PEG400 can inhibit Fe–B nanoparticles from agglomeration. They found that during the FTS reaction, Fe–B converted to α-Fe first, followed by carbonization and oxidation to iron carbides and Fe_3O_4, respectively. Among the catalysts reduced in solvents with different EG/water ratios, the Fe–B reduced in water exhibited the highest activity of 0.83 mol_{CO} mol_{Fe}^{-1} h^{-1}.[263] Spherical and rod-like Fe–B nanoparticles prepared in W/O microemulsions displayed a high CO conversion of *ca.* 80% at 473 K after 12 h reaction in PEG400, while the selectivity to heavier hydrocarbons on the rod-like catalyst is slightly higher.[91] Fe–B nanoclusters of ~8 nm showed higher activity of 1.5 mol_{CO} mol_{Fe}^{-1} h^{-1} than Co–B at 423 K in PEG200.[259] When the FTS reaction was carried out in EG,[260] Fe–B gave a much higher activity of 0.68 mol_{CO} mol_{Fe}^{-1} h^{-1} than Co–B, and selectivities to dioxolanes of 68 wt% and hydrocarbons of 26 wt%, showing that Fe–B is more favorable for the synthesis of dioxolanes. Interestingly, these results demonstrate that Fe–B nanoparticles can be more active than Co–B nanoparticles in low-temperature FTS reaction, in sharp contrast to the performances of those metals in crystalline form above 473 K.[255]

5.7 Application in other reactions

5.7.1 Hydrogenolysis of ethyl lactate. 1,2-Propanediol (1,2-PDO) is useful for the production of polyester resins, polymers, pharmaceuticals, and functional fluids (antifreeze, deicing). Ethyl lactate, as one of the biomass-derived organic molecules, can be produced by fermentation of a number of renewable resources.[264] Hydrogenation of ethyl lactate provides a green process to 1,2-PDO and thus attracts much attention.[265] However, high reaction temperature should be avoided, since the reactive hydroxyl group in ethyl lactate tends to undergo side reactions, leading to a drop in 1,2-PDO selectivity (Scheme 11).[84] Accordingly, developing catalysts active under mild reaction conditions is crucial for the transformation of ethyl lactate to 1,2-PDO.

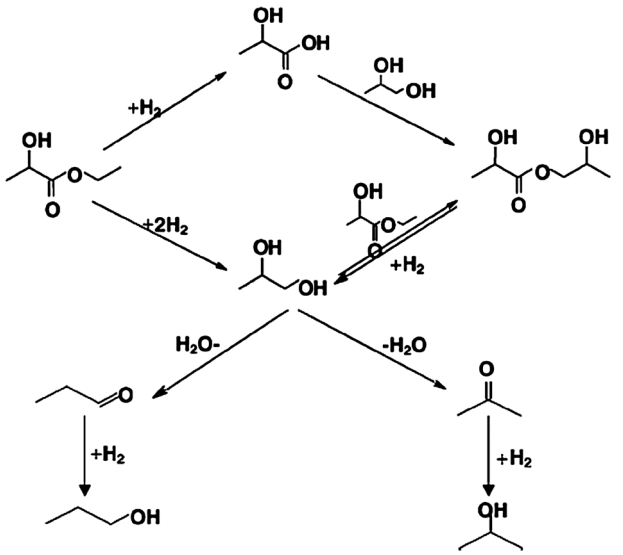

Scheme 11 Possible reaction pathway in the hydrogenation of ethyl lactate. Reproduced from ref. 84 with kind permission from Elsevier.

A leading work on the hydrogenation of ethyl lactate to 1,2-PDO over amorphous alloy catalysts (Ru–Sn–B/γ-Al_2O_3) was conducted by Yan and coworkers.[84] Addition of a suitable amount of Sn to Ru–B significantly increased the ethyl lactate conversion and 1,2-PDO selectivity. The 1,2-PDO selectivity reached 92% at an ethyl lactate conversion of 91% under mild reaction conditions. On Ru–B/Sn-SBA-15 (Si/Sn molar ratio 30), the 1,2-PDO selectivity of 99% was obtained at an ethyl lactate conversion of 68%.[266] On Ru–B/TiO_2, the 1,2-PDO selectivity of above 95% at ethyl lactate conversion of 98% was reported under even milder reaction conditions.[267]

5.7.2 Dehydrogenation. Dehydrogenation of alcohols can produce the corresponding aldehydes and ketones, as well as H_2 and esters.[268–270] The catalysts for this reaction involve Cu,[271] Fe,[272] and noble metals like Au,[273] Pd,[274] Ir,[270] Ag,[275] Os, and Ru.[276] Chen and coworkers investigated the dehydrogenation of ethanol to acetaldehyde on Fe-based amorphous alloy catalysts.[272,277,278] $Fe_{72.8}B_{27.2}$ and $Fe_{89.1}P_{10.9}$ showed high activity and nearly 100% selectivity.[272,277] Moreover, Fe–P–B exhibited higher weight specific activity than Fe–P and Fe–B.[278]

5.7.3 Oxidation. Oxidation of CO has attracted much attention because of its relevance to many industrial applications.[279] Over the Pt/Co–B/TiO_2 catalyst, the CO conversion is 86%, which is much higher than the conversion of 39% on Pt/Co/TiO_2 under the same reaction conditions.[280] A large number of works have been focused on the partial oxidation of CH_4 (POM) to syngas,[281–284] since the product is useful for FTS and methanol production.[285] In POM, the Ca-decorated

γ-Al_2O_3(Ca–AlO)-supported low-Ni loading (<1 wt%) Ni–B catalysts exhibited high activity and selectivity comparable to those on 10 wt% Ni/γ-Al_2O_3 and 1 wt% Rh/γ-Al_2O_3.[286] Moreover, the coke deposition on Ni–B/Ca–AlO is much lower than that on 10 wt% Ni/γ-Al_2O_3 due to the structural effect of B.

Due to the low cost, improved safety, and low reaction pressure, the synthesis of H_2O_2 from CO, H_2O and O_2 is more promising than the eAQ route and direct synthesis of H_2O_2 from H_2 and O_2.[52] Ni–La–B/γ-Al_2O_3 showed a H_2O_2 production rate of 0.07 mmol $g_{cat.}^{-1}$ h^{-1} from CO, H_2O and O_2, which is comparable to the rate on 5% Pd/$CaCO_3$ and 1% Ru/graphite (0.1 mmol $g_{cat.}^{-1}$ h^{-1}).[287–289] Ni–P–B/Al_2O_3 exhibited higher activity and stability than those noble metal catalysts, giving a H_2O_2 production rate of as high as 0.228 mmol $g_{cat.}^{-1}$ h^{-1}.[52]

5.7.4 One-step hydrogenation of phenol to cyclohexanone. Cyclohexanone is a highly important industrial feedstock for manufacturing caprolactam and adipic acid, which are intermediates for nylon 6 and nylon 66, respectively. In comparison with the traditional routes for cyclohexanone production from the oxidation of cyclohexane,[290] and the hydrogenation of phenol to cyclohexanol followed by dehydrogenation,[291] one-step hydrogenation of phenol to cyclohexanone is more concise, environmentally more friendly, and more energy-efficient.[292] The reaction route is illustrated in Scheme 12. Li and coworkers investigated the hydrogenation of phenol to cyclohexanone on Pd–B amorphous alloy catalysts.[293–295] The La- or Ce-doped Pd–B catalyst exhibited higher activity and selectivity to cyclohexanone than the undoped Pd–B, and the maximum cyclohexanone yields over Pd–La–B (La/(Pd + La + B) molar ratio = 1%) and Pd–Ce–B (Ce/Pd molar ratio = 0.44%) are 79% and 83%, respectively.[293,295] The properties of the supports influence the catalytic performance of the Pd–B catalyst.[295] The phenol conversion and cyclohexanone selectivity at the maximum cyclohexanone yield over the 5.8% Pd–Ce–B/MgAl hydrotalcite (HT) are 82% and 80%, respectively, superior to the values on the Al_2O_3-, MgO-, and SiO_2-supported catalysts.

5.7.5 Reduction of *N*-nitrosodimethylamine (NDMA). NDMA, a probable human carcinogen, has been recently detected as a contaminant in drinking and ground water.[296] Traditional physicochemical treatment technologies are inefficient to eliminate NDMA, and ultraviolet treatment is efficient but uneconomical.[297] Powdered metal catalysts like Pd and Ni in the presence of H_2 present notable potential for rapid destruction

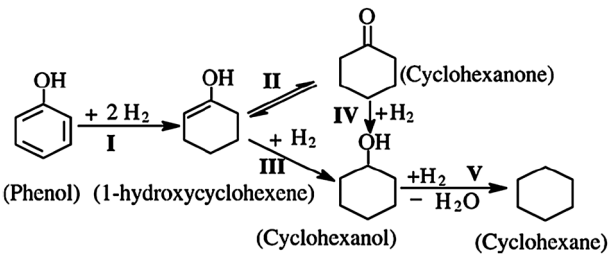

Scheme 12 A plausible reaction mechanism for phenol hydrogenation. Reproduced from ref. 295 with kind permission from Elsevier.

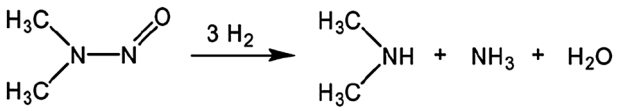

Scheme 13 Reduction of NDMA on the Ni–B catalyst. Reproduced from ref. 55 with kind permission from Elsevier.

of NDMA in water[296] Strathmann and coworkers reported that Ni–B exhibited higher intrinsic activity than RANEY® Ni in the reduction of NDMA (Scheme 13).[55] The activity of Ni–B was not affected by solution pH and extended exposure of the dry catalyst to air, while RANEY® Ni immediately deactivated by exposure to air. Ni–B is also more tolerant to dissolved oxygen and low concentration of dissolved sulfide than RANEY® Ni, showing its great potential in eliminating NDMA in water.

5.7.6 Hydroamination of phenylpyruvic acid (PPA). Phenylalanine (Phe) is widely used in pabulum and pharmaceutical industries, for instance, as an amino acid infusion[298] and as a precursor for manufacturing aspartame.[299] Chemical synthesis of Phe from PPA hydroamination has attracted much attention, since PPA can be easily obtained *via* double carbonylation of benzyl chloride.[300] Ni–B/SiO_2 is effective for the synthesis of Phe from PPA by amination and hydrogenation (Scheme 14).[54] On this catalyst, the selectivity and yield of Phe are 99% and 98%, respectively, both of which are higher than those on Urushibara Ni (U–Ni) and RANEY® Ni.

5.7.7 Barbier-type carbonyl allylation. Synthesis of homoallylic alcohols *via* Barbier-type carbonyl allylation is of great importance, since the homoallylic alcohols are versatile subunits for manufacturing many useful biologically active molecules including polyether, macrolides, and antibiotics.[301] The Barbier-type carbonyl allylation has been realized mainly by homogeneous organometallic catalysis.[302,303] The Barbier-type carbonyl allylation in aqueous media was realized on metallic In powder in 1991.[304] The In powder exhibited high selectivity, but with lower efficiency compared to the homogeneous catalysts. Li and coworkers reported that the In–B amorphous alloy showed higher activity than the In powder in allylation of benzaldehyde in water, and maintained a high selectivity of 98% (Scheme 15).[305] They further demonstrated that In–B is active for the Barbier-type allylation of substituted benzaldehydes and a number of allylic halides with selectivities $\geq$ 97% at conversions $\geq$ 94%. In Barbier-type allylation of acetophenone on In–B, allyl bromide showed similar allylation result to the expensive allylboronate, giving the 2-phenyl-4-penten-2-ol selectivity of 94% at the conversion of 90%.

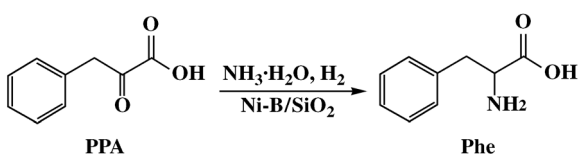

Scheme 14 The route for the synthesis of Phe. Reproduced from ref. 54 with kind permission from Elsevier.

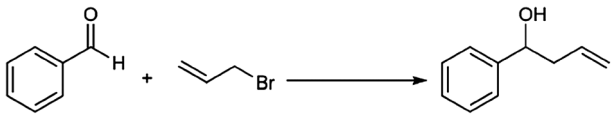

Scheme 15 Barbier-type allylation of benzaldehyde with allyl bromide.

6. Conclusions

The importance of amorphous alloys in catalysis has attracted the rapid expansion of research on the synthesis and catalysis of chemically reduced metal–metalloid amorphous alloy catalysts. Various synthetic strategies, transplanted from newly emerged methods[115–117,121–125,129–132] or characteristic of the chemical reduction method,[53,90,91,128] have been developed to prepare size-, morphology-, or texture-specific metal–metalloid amorphous alloy catalysts. New supports, such as regular mesoporous molecular sieves and CNTs, have been used to improve the dispersion and thermal stability of the amorphous alloy nanoparticles. Incorporation of a promoter, in the oxidized or metallic state, structurally or electronically modifies the physical characters of the amorphous alloy catalysts in terms of dimension, thermal stability, and electron density, which further tune the catalytic performance. In a number of catalytic reactions in petrochemistry, energy conversion, and environmental remediation, metal–metalloid amorphous alloys exhibit impressive catalytic performance. High or exclusive selectivities to targeting products were reported on some amorphous alloy catalysts. Amorphous alloy catalysts are usually more active than their crystalline counterparts and catalysts reduced by H_2. In certain cases, non-noble metal-based amorphous alloy catalysts even exhibited higher activity than noble metal catalysts. In addition, a few investigations suggested that amorphous alloys can function as precursors of high-performance catalysts upon proper pretreatment. These striking results, in conjugation with the easiness of the chemical reduction method to synthesize metal–metalloid amorphous alloys with desired combinations and contents of metal and metalloid, show promise for amorphous alloy catalysts as efficient and economical alternatives to traditional RANEY® Ni and Pd/C catalysts widely used in the chemical industry. In particular, industrial applications of metal–metalloid amorphous alloy catalysts will be most probably realized in the saturation of olefinic bonds, carbonyl groups, and nitro groups that can readily occur on these high-performance catalysts. Partial hydrogenation of benzene and chemoselective hydrogenation of conjugated unsaturated aldehydes or ketones are another two kinds of reactions that are promising for amorphous alloy catalysts to act as industrial catalysts owing to their outstanding selectivities. For further investigations, much attention may be paid to the exploration of the catalytic performance of metal–metalloid amorphous alloy catalysts in more complicated and value-added reactions such as enantioselective hydrogenation and the synthesis of pharmaceutical intermediates.

On the other hand, in most cases the catalytic performance of the metal–metalloid amorphous alloy catalysts is simply explained by the electronic effect due to the bond formation between metal and metalloid. There are very limited studies aiming to establish an in-depth understanding of the structure–performance relationship on amorphous alloy catalysts. This surprising falling-behind as compared to the rapid progress in their synthesis and catalytic applications can be mainly explained by the amorphous structure inaccessible to conventional XRD, TEM and SAED techniques, which are only suitable for extracting structural information of crystalline materials. In this respect, more attention should be paid to synchrotron- or neutron-based techniques powerful in revealing the structural mysteries of amorphous alloys of various compositions toward understanding of catalytic mechanisms on amorphous alloys. However, it should be noted that these techniques only provide structure-averaged information, while the possibility exists that the amorphous alloy is constructed by one or more types of atomic clusters. Thus, a close cooperation with theoretical modeling will be instructive to the establishment of an accurate structure–performance relationship over amorphous alloy catalysts.

As compared to the vast abundance of the reactions investigated on metal–metalloid amorphous alloy catalysts, information about the surface chemistry of this type of catalysts is lacking at the molecular level. Investigation of the adsorption strength, adsorption mode, and the reaction intermediate of the reactants on the amorphous alloy catalysts is important to elucidate the difference in the catalytic performance between amorphous and crystalline catalysts.

A vacuum approach of surface science is widely used for fundamental studies of surface adsorption, dissociation, and desorption. Due to the limit of inelastic mean free paths of electrons at ambient pressure, so far most electron-based surface analysis techniques can only be used to study surface chemistry and structure under high vacuum or ultrahigh vacuum. Thus, most studies using such techniques are performed with an approach called *ex situ* studies. This approach uses well-defined single crystals as model catalysts. It provides insights toward understanding the catalytic mechanism at the molecular level though a pressure gap and a materials gap were raisen in recent decade. In the case of amorphous alloy catalysts, the vacuum approach faces an additional challenge. Conventional *ex situ* studies demand a sputtering–annealing treatment of model catalysts to prepare a clean surface before *ex situ* studies. Since amorphous alloys are thermodynamically metastable, when subjected to such a harsh treatment, they are inclined to undergo structure transformation or crystallization, thus losing their pristine structural character. In this connection, *in situ* or Operando characterization techniques[306,307] are essential for providing meaningful information on the adsorption and reaction of the reactants on amorphous alloy catalysts, which will facilitate a rational design of amorphous catalysts with desired performance.

To improve the operation longevity of the metastable metal–metalloid amorphous alloy catalysts, endeavors have been focused predominantly on catalyst preparation. Dispersing amorphous alloy nanoparticles on a high-surface area or high-porosity support, and modifying the amorphous alloy with selected element are effective ways to sustain the amorphous structure to as high as 600 K or above. Combined with the excellent low-temperature catalytic activity of the amorphous alloys, apparently the improved T_c can meet the temperature

requirement of many reactions. However, to ensure a long-term operation, reaction temperature as low as possible is preferred, since the amorphous alloy may undergo slow but irreversible structure relaxation even below T_c. Reaction engineering technology can be intriguing, but has long been ignored, to prolong the lifetime of the amorphous alloy catalysts. One promising reactor type for metal–metalloid amorphous alloy catalysts is the magnetically stabilized-bed (MSB) reactor.[308] This reactor is conductive to good mass and heat transportations, and fine and friable catalyst particles can be used free from high pressure drop.[309] For example, for a skeletal Ni catalysts, the optimal temperature for CO methanation on the MSB reactor was markedly lowered by *ca.* 100 K as compared to the same catalyst on the conventional fixed-bed reactor.[310] Thus, integrating the advantages of the metal–metalloid amorphous alloy catalysts and the MSB reactor or other adequate type of reactor will surely advance the industrial application of the amorphous alloy catalysts in various chemical processes.

Acknowledgements

This work was supported by the National Basic Research Program of China (2012CB224804), the NSF of China (21073043), the Science & Technology Commission of Shanghai Municipality (10JC1401800, 08DZ2270500), the Program of New Century Excellent Talents (NCET-08-0126), the Key Laboratory of Resource Chemistry of Ministry of Education, Shanghai Normal University, the Chemical Sciences, Geosciences and Biosciences Division, Office of Basic Energy Sciences, Office of Science, U.S. Department of Energy under the grant DE-FG02-12ER1635, and ACS PRF, and the startup funds from University of Notre Dame and seed funds from Center for Sustainable Energy at Notre Dame.

Notes and references

1 M. H. Bhat, V. Molinero, E. Soignard, V. C. Solomon, S. Sastry, J. L. Yarger and C. A. Angell, *Nature*, 2007, **448**, 787.
2 D. B. Miracle, *Nat. Mater.*, 2004, **3**, 697.
3 F. E. Luborsky, *Amorphous Metallic Alloys*, Butterworths, London, 1983.
4 Z. Hu, Y. Fan and Y. Chen, *Appl. Phys. A: Mater. Sci. Process.*, 1999, **68**, 225.
5 W. H. Wang, *Nat. Mater.*, 2012, **11**, 275.
6 H. Zahn and J. Kramer, *Z. Phys.*, 1933, **86**, 413.
7 G. V. Smith, W. E. Brower, Jr and M. S. Matyjaszczyk, *7th Proc. Int. Congr. Catal.*, 1980, 355.
8 J. van Wonterghem, S. Mørup, C. J. W. Koch, S. W. Charles and S. Wells, *Nature*, 1986, **322**, 622.
9 H. I. Schlesinger, H. C. Brown, A. E. Finholt, J. R. Gilbreath, H. Hoekstra and E. K. Hyde, *J. Am. Chem. Soc.*, 1953, **75**, 215.
10 Á. Molnár, M. Bartók and G. V. Smith, *Adv. Catal.*, 1989, **36**, 329.
11 A. Baiker, *Faraday Discuss. Chem. Soc.*, 1989, **87**, 239.
12 A. M. Argo, J. F. Odzak, F. S. Lai and B. C. Gates, *Nature*, 2002, **415**, 623.
13 J. M. Thomas, *J. Chem. Phys.*, 2008, **128**, 182502.
14 J. M. Thomas, B. F. G. Johnson, R. Raja, G. Sankar and P. A. Midgley, *Acc. Chem. Res.*, 2003, **36**, 20.
15 J. M. Thomas, *Top. Catal.*, 2008, **50**, 98.
16 J. M. Thomas and R. Raja, *Top. Catal.*, 2010, **53**, 848.
17 J. M. Thomas, Z. Saghi and P. L. Gai, *Top. Catal.*, 2011, **54**, 588.
18 J. M. Thomas, *Proc. R. Soc. London, Ser. A*, 2012, **468**, 1884.
19 W. E. Brower Jr, M. S. Matyjaszczyk, T. L. Pettit and G. V. Smith, *Nature*, 1983, **301**, 497.
20 S. Yoshida, H. Yamashita, T. Funabiki and T. Yonezawa, *J. Chem. Soc., Faraday Trans. 1*, 1984, **80**, 1435.
21 Y. Chen, *Catal. Today*, 1998, **44**, 3.
22 J. F. Deng, H. X. Li and W. J. Wang, *Catal. Today*, 1999, **51**, 113.
23 J. F. Deng and H. Y. Chen, *J. Mater. Sci. Lett.*, 1993, **12**, 1508.
24 S. Linderoth and S. Mørup, *J. Appl. Phys.*, 1990, **67**, 4472.
25 S. Linderoth and S. Mørup, *J. Appl. Phys.*, 1991, **69**, 5256.
26 J. Y. Shen, Z. Y. Li, Y. N. Fan, Z. Hu and Y. Chen, *J. Solid State Chem.*, 1993, **106**, 493.
27 J. Y. Shen, Z. Y. Li, Q. J. Yan and Y. Chen, *J. Phys. Chem.*, 1993, **97**, 8504.
28 Z. Liu, W. L. Dai, B. Liu and J. F. Deng, *J. Catal.*, 1999, **187**, 253.
29 Y. G. He, M. H. Qiao, H. R. Hu, Y. Pei, H. X. Li, J. F. Deng and K. N. Fan, *Mater. Lett.*, 2002, **56**, 952.
30 H. X. Li, H. Li, W. L. Dai and M. H. Qiao, *Appl. Catal., A*, 2003, **238**, 119.
31 S. H. Xie, M. H. Qiao, W. Z. Zhou, G. Luo, H. Y. He, K. N. Fan, T. J. Zhao and W. K. Yuan, *J. Phys. Chem. B*, 2005, **109**, 24361.
32 S. Wells, S. W. Charles, S. Mørup, S. Linderoth, J. van Wonterghem, J. Larsen and M. B. Madsen, *J. Phys.: Condens. Matter*, 1989, **1**, 8199.
33 W. L. Dai, M. H. Qiao and J. F. Deng, *Appl. Surf. Sci.*, 1997, **120**, 119.
34 Z. B. Yu, M. H. Qiao, H. X. Li and J. F. Deng, *Appl. Catal., A*, 1997, **163**, 1.
35 J. Y. Shen, Z. Hu, Y. F. Hsia and Y. Chen, *Appl. Phys. Lett.*, 1991, **59**, 2510.
36 J. Y. Shen, Z. Hu, Q. Zhang, L. F. Zhang and Y. Chen, *J. Appl. Phys.*, 1992, **71**, 5217.
37 J. F. Deng, X. P. Zhang and E. Z. Min, *Appl. Catal.*, 1988, **37**, 339.
38 K. Hashimoto, *Mater. Sci. Eng., A*, 1997, **226–228**, 891.
39 S. Q. Wei, H. Oyanagi, Z. R. Li, X. Y. Zhang, W. H. Liu, S. L. Yin and X. G. Wang, *Phys. Rev. B: Condens. Matter Mater. Phys.*, 2001, **63**, 224201.
40 Z. Jiang, H. W. Yang, Z. Wei, Z. Xie, W. J. Zhong and S. Q. Wei, *Appl. Catal., A*, 2005, **279**, 165.
41 Y. Pei, P. J. Guo, M. H. Qiao, H. X. Li, S. Q. Wei, H. Y. He and K. N. Fan, *J. Catal.*, 2007, **248**, 303.
42 Z. Wei, Z. R. Li, Z. Jiang, J. Ye, W. J. Zhong, J. X. Song and S. Q. Wei, *J. Alloys Compd.*, 2008, **460**, 553.
43 M. S. Nashner, A. I. Frenkel, D. Somerville, C. W. Hills, J. R. Shapley and R. G. Nuzzo, *J. Am. Chem. Soc.*, 1998, **120**, 8093.
44 J. H. Kang, L. D. Menard, R. G. Nuzzo and A. I. Frenkel, *J. Am. Chem. Soc.*, 2006, **128**, 12068.
45 J. F. Geng, D. A. Jefferson and B. F. G. Johnson, *Chem. Commun.*, 2007, 969.
46 B. J. Liaw and Y. Z. Chen, *Appl. Catal., A*, 2001, **206**, 245.
47 Y. Z. Chen, B. J. Liaw and B. J. Chen, *Appl. Catal., A*, 2002, **236**, 121.
48 P. J. Guo, L. F. Chen, S. R. Yan, W. L. Dai, M. H. Qiao, H. L. Xu and K. N. Fan, *J. Mol. Catal. A: Chem.*, 2006, **256**, 164.
49 Y. Z. Chen and Y. C. Chen, *Appl. Catal., A*, 1994, **115**, 45.
50 H. X. Li, Y. D. Wu, H. S. Luo, M. H. Wang and Y. P. Xu, *J. Catal.*, 2003, **214**, 15.
51 Y. C. Liu and Y. W. Chen, *Ind. Eng. Chem. Res.*, 2006, **45**, 2973.
52 Z. L. Ma, S. K. Jiang, L. Zhang and C. Q. Liu, *Appl. Catal., A*, 2006, **311**, 34.
53 S. J. Chiang, B. J. Liaw and Y. Z. Chen, *Appl. Catal., A*, 2007, **319**, 144.
54 Q. F. Liang, A. Q. Zhang and L. Li, *J. Nat. Gas Chem.*, 2008, **17**, 303.
55 A. J. Frierdich, C. E. Joseph and T. J. Strathmann, *Appl. Catal., B*, 2009, **90**, 175.
56 Y. Okamoto, Y. Nitta, T. Imanaka and S. Teranishi, *J. Chem. Soc., Faraday Trans. 1*, 1979, **15**, 2027.
57 Y. Okamoto, Y. Nitta, T. Imanaka and S. Teranishi, *J. Catal.*, 1980, **64**, 397.
58 T. Imanaka, J. Tamaki and S. Teranishi, *Chem. Lett.*, 1984, 449.
59 J. Tamaki and T. Imanaka, *Chem. Lett.*, 1986, 679.
60 W. S. Xia, Y. Fan, Y. S. Jiang and Y. Chen, *Appl. Surf. Sci.*, 1996, **103**, 1.
61 J. F. Deng, H. Y. Chen, X. H. Bao and M. Muhler, *Appl. Surf. Sci.*, 1994, **81**, 341.
62 H. Li, H. X. Li, W. L. Dai, W. J. Wang, Z. G. Fang and J. F. Deng, *Appl. Surf. Sci.*, 1999, **152**, 25.
63 L. Finney, *Nature*, 1977, **266**, 309.
64 J. Li, M. H. Qiao and J. F. Deng, *J. Mol. Catal. A: Chem.*, 2001, **169**, 295.

65 H. B. Guo, H. X. Li, J. Zhu, W. H. Ye, M. H. Qiao and W. L. Dai, *J. Mol. Catal. A: Chem.*, 2003, **200**, 213.
66 S. Diplas, J. Lehrmann, S. Jørgensen, T. Våland and J. Taftø, *Philos. Mag.*, 2005, **85**, 981.
67 S. Diplas, S. Jørgensen, J. Taftø, T. Tønnessen, T. Knutsen, J. Lehrmann, T. Våland, M. L. Abel and J. F. Watts, *Surf. Interface Anal.*, 2006, **38**, 238.
68 S. Diplas and O. M. Løvvik, *J. Phys.: Condens. Matter*, 2009, **21**, 245503.
69 S. N. Ishmaev, S. L. Isakov, I. P. Sadikov and E. Svab, *J. Non-Cryst. Solids*, 1987, **94**, 11.
70 T. A. Weber and F. H. Stillinger, *Phys. Rev. B: Condens. Matter Mater. Phys.*, 1985, **31**, 1954.
71 Z. G. Fang, B. R. Shen, J. Lu, K. N. Fan and J. F. Deng, *Acta Chim. Sin. (Engl. Ed.)*, 1999, **57**, 894.
72 Z. G. Fang, B. R. Shen, K. N. Fan and J. F. Deng, *Acta Chim. Sin. (Engl. Ed.)*, 1999, **57**, 1246.
73 Z. G. Fang, B. R. Shen and K. N. Fan, *Chin. J. Chem. Phys.*, 2002, **15**, 17.
74 Z. G. Fang, K. N. Fan and H. L. Jiang, *Chin. J. Chem. Phys.*, 2004, **17**, 684.
75 Q. S. Zeng, W. K. Chen, Y. F. Zhang, W. X. Dai and X. Guo, *J. Nat. Gas Chem.*, 2010, **19**, 300.
76 Q. S. Zeng, W. K. Chen, W. X. Dai, Y. F. Zhang, Y. Li and X. Guo, *Chin. J. Catal.*, 2010, **31**, 423.
77 M. H. Qiao, S. H. Xie, W. L. Dai and J. F. Deng, *Catal. Lett.*, 2001, **71**, 187.
78 B. R. Shen, S. Q. Wei, K. N. Fan and J. F. Deng, *Appl. Phys. A: Mater. Sci. Process.*, 1997, **65**, 295.
79 L. F. Chen and Y. W. Chen, *Ind. Eng. Chem. Res.*, 2006, **45**, 8866.
80 X. F. Chen, H. X. Li, H. S. Luo and M. H. Qiao, *Appl. Catal., A*, 2002, **233**, 13.
81 H. X. Li, S. Y. Zhang and H. S. Luo, *Mater. Lett.*, 2004, **58**, 2741.
82 S. Q. Wei, H. Y. Cui, J. H. Wang, S. P. Zhuo, W. M. Yi, L. H. Wang and Z. H. Li, *Particuology*, 2011, **9**, 69.
83 J. Fang, X. Y. Chen, B. Liu, S. R. Yan, M. H. Qiao, H. X. Li, H. Y. He and K. N. Fan, *J. Catal.*, 2005, **229**, 97.
84 G. Luo, S. R. Yan, M. H. Qiao, J. H. Zhuang and K. N. Fan, *Appl. Catal., A*, 2004, **275**, 95.
85 B. J. Liaw, C. H. Chen and Y. Z. Chen, *Chem. Eng. J.*, 2010, **157**, 140.
86 H. X. Li, H. S. Luo, L. Zhuang, W. L. Dai and M. H. Qiao, *J. Mol. Catal. A: Chem.*, 2003, **203**, 267.
87 X. H. Yan, J. Q. Sun, Y. W. Wang and J. F. Yang, *J. Mol. Catal. A: Chem.*, 2006, **252**, 17.
88 C. Luo, W. N. Wang, M. H. Qiao and K. N. Fan, *J. Mol. Catal. A: Chem.*, 2002, **184**, 379.
89 D. Acosta, N. Ramírez, E. Erdmann, H. Destéfanis and E. Gonzo, *Catal. Today*, 2008, **133–135**, 49.
90 H. Li, J. Liu, S. H. Xie, M. H. Qiao, W. L. Dai and H. X. Li, *J. Catal.*, 2008, **259**, 104.
91 X. F. Cheng, B. S. Wu, Y. Yang and Y. W. Li, *Catal. Commun.*, 2011, **12**, 431.
92 B. J. Liaw, S. J. Chiang, C. H. Tsai and Y. Z. Chen, *Appl. Catal., A*, 2005, **284**, 239.
93 J. Bu, J. Q. Wang, M. H. Qiao, S. R. Yan, H. X. Li and K. N. Fan, *Acta Chim. Sin. (Engl. Ed.)*, 2007, **65**, 1338.
94 B. J. Liaw, S. J. Chiang, S. W. Chen and Y. Z. Chen, *Appl. Catal., A*, 2008, **346**, 179.
95 H. Li, C. J. Ma and H. X. Li, *Chin. J. Chem.*, 2006, **24**, 613.
96 H. X. Li, H. Li, J. Zhang, W. L. Dai and M. H. Qiao, *J. Catal.*, 2007, **246**, 301.
97 H. Li, J. Zhang and H. X. Li, *Catal. Commun.*, 2007, **8**, 2212.
98 H. Li, Y. Wang, Q. F. Zhao and H. X. Li, *Res. Chem. Intermed.*, 2009, **35**, 779.
99 G. Y. Bai, L. B. Niu, M. D. Qiu, F. He, X. X. Fan, H. Y. Dou and X. F. Zhang, *Catal. Commun.*, 2010, **12**, 212.
100 A. Roucoux, J. Schulz and H. Patin, *Chem. Rev.*, 2002, **102**, 3757.
101 H. Goesmann and C. Feldmann, *Angew. Chem., Int. Ed.*, 2010, **49**, 1362.
102 K. S. Suslick, *Science*, 1990, **247**, 1439.
103 K. S. Suslick, S. B. Choe, A. A. Cichowlas and M. W. Grinstaff, *Nature*, 1991, **353**, 414.
104 N. A. Dhas and A. Gedanken, *Chem. Mater.*, 1997, **9**, 3144.
105 L. H. Thompson and L. K. Doraiswamy, *Ind. Eng. Chem. Res.*, 1999, **38**, 1215.
106 S. Devarakonda, J. M. B. Evans and A. S. Myerson, *Cryst. Growth Des.*, 2003, **3**, 741.
107 T. Prozorov, R. Prozorov and K. S. Suslick, *J. Am. Chem. Soc.*, 2004, **126**, 13890.
108 Y. F. Lu, H. Y. Fan, A. Stump, T. L. Ward, T. Rieker and C. J. Brinker, *Nature*, 1999, **398**, 223.
109 J. N. Cha, G. D. Stucky, D. E. Morse and T. J. Deming, *Nature*, 2000, **403**, 289.
110 S. W. Kim, M. Kim, W. Y. Lee and T. Hyeon, *J. Am. Chem. Soc.*, 2002, **124**, 7642.
111 X. Y. Chen, W. L. Yang, S. Wang, M. H. Qiao, S. R. Yan, K. N. Fan and H. Y. He, *New J. Chem.*, 2005, **29**, 266.
112 G. W. Xie, Z. G. Lu, Z. B. Wang and Z. L. Cui, *Catal. Commun.*, 2008, **9**, 1766.
113 S. Wang, W. L. Yang, G. B. Yu, S. H. Xie, M. H. Qiao and K. N. Fan, *Chin. J. Chem.*, 2008, **26**, 1191.
114 X. L. Zhang, J. H. Liu and S. M. Li, *Mater. Lett.*, 2009, **63**, 1907.
115 H. Li, Y. Xu, J. Liu, Q. F. Zhao and H. X. Li, *J. Colloid Interface Sci.*, 2009, **334**, 176.
116 Y. Zhu, F. P. Liu, W. P. Ding, X. F. Guo and Y. Chen, *Angew. Chem., Int. Ed.*, 2006, **45**, 7211.
117 W. P. Ding, X. F. Guo, M. Mo, Y. Zhu and Y. Chen, *Chin. J. Catal.*, 2010, **31**, 887.
118 C. T. Kresge, M. E. Leonowicz, W. J. Roth, J. C. Vartuli and J. S. Beck, *Nature*, 1992, **359**, 710.
119 D. Y. Zhao, J. Feng, Q. S. Huo, N. Melosh, G. H. Fredrickson, B. F. Chmelka and G. D. Stucky, *Science*, 1998, **279**, 548.
120 H. Li, H. X. Yang and H. X. Li, *J. Catal.*, 2007, **251**, 233.
121 Q. Meng, H. Li and H. X. Li, *J. Phys. Chem. C*, 2008, **112**, 11448.
122 H. X. Li, Q. F. Zhao, Y. Wan, W. L. Dai and M. H. Qiao, *J. Catal.*, 2006, **244**, 251.
123 D. G. Tong, X. Han, W. Chu, H. Chen and X. Y. Ji, *Mater. Lett.*, 2007, **61**, 4679.
124 D. G. Tong, W. Chu, Y. Y. Luo, H. Chen and X. Y. Ji, *J. Mol. Catal. A: Chem.*, 2007, **269**, 149.
125 H. Li, D. Q. Zhang, G. S. Li, Y. Xu, Y. F. Lu and H. X. Li, *Chem. Commun.*, 2010, **46**, 791.
126 F. Gao, Q. Y. Lu and D. Y. Zhao, *Adv. Mater.*, 2003, **15**, 739.
127 A. H. Lu and F. Schüth, *Adv. Mater.*, 2006, **18**, 1793.
128 X. Y. Chen, Z. Y. Lou, S. H. Xie, M. H. Qiao, S. R. Yan, Y. L. Zhu, K. N. Fan and H. Y. He, *Chem. Lett.*, 2006, 390.
129 Q. H. Wang, L. F. Jiao, H. M. Du, D. W. Song, W. X. Peng, Y. C. Si, Y. J. Wang and H. T. Yuan, *Electrochim. Acta*, 2010, **55**, 7199.
130 Z. J. Yan and D. S. Xue, *J. Mater. Sci.*, 2008, **43**, 771.
131 N. Patel, R. Fernandes, G. Guella, A. Kale, A. Miotello, B. Patton and C. Zanchetta, *J. Phys. Chem. C*, 2008, **112**, 6968.
132 N. Patel, R. Fernandes, G. Guella and A. Miotello, *Appl. Catal., B*, 2010, **95**, 137.
133 H. Li, C. Z. Wang, Q. F. Zhao and H. X. Li, *Appl. Surf. Sci.*, 2008, **254**, 7516.
134 B. Liu, M. H. Qiao, J. Q. Wang, S. H. Xie, H. X. Li and K. N. Fan, *J. Chem. Technol. Biotechnol.*, 2003, **78**, 512.
135 Z. J. Wu, S. H. Ge, M. H. Zhang, W. Li and K. Y. Tao, *Catal. Commun.*, 2008, **9**, 1432.
136 R. Dagani, *Chem. Eng. News*, 1997, **75**, 26.
137 W. J. Wang, M. H. Qiao, J. Yang, S. H. Xie and J. F. Deng, *Appl. Catal., A*, 1997, **163**, 101.
138 W. J. Wang, M. H. Qiao, H. X. Li, W. L. Dai and J. F. Deng, *Appl. Catal., A*, 1998, **168**, 151.
139 Y. G. He, M. H. Qiao, H. R. Hu, J. F. Deng and K. N. Fan, *Appl. Catal., A*, 2002, **228**, 29.
140 H. Yan, W. Li, M. H. Zhang and K. Y. Tao, *Chin. J. Catal.*, 2009, **30**, 89.
141 L. Wang, W. Li, M. H. Zhang and K. Y. Tao, *Appl. Catal., A*, 2004, **259**, 185.
142 G. O. Mallory and J. B. Hajdu, *Electroless Plating: Fundamentals and Applications*, American Electroplaters and Surface Finishers Society, Orlando, 1990.
143 Z. J. Wu, S. H. Ge, M. H. Zhang, W. Li, S. C. Mu and K. Y. Tao, *J. Phys. Chem. C*, 2007, **111**, 8587.
144 S. H. Ge, Z. J. Wu, M. H. Zhang, W. Li and K. Y. Tao, *Ind. Eng. Chem. Res.*, 2006, **45**, 2229.
145 H. L. Wen, K. S. Yao, J. Wei, Z. M. Zhou and A. Kirschning, *J. Nanopart. Res.*, 2009, **11**, 499.

146 C. Q. Xu, D. J. Zhu and G. X. Li, *J. Funct. Mater.*, 2004, **35**, 1974.
147 R. F. Nystrom, *J. Am. Chem. Soc.*, 1955, **77**, 2544.
148 S. Caddick, A. K. de K. Haynes, D. B. Judd and M. R. V. Williams, *Tetrahedron Lett.*, 2000, **41**, 3513.
149 A. Rahman and S. B. Jonnalagadda, *Catal. Lett.*, 2008, **123**, 264.
150 A. Rahman and S. B. Jonnalagadda, *J. Mol. Catal. A: Chem.*, 2009, **299**, 98.
151 A. Corma, *Chem. Rev.*, 1997, **97**, 2373.
152 S. T. Wong, J. F. Lee, J. M. Chen and C. Y. Mou, *J. Mol. Catal. A: Chem.*, 2001, **165**, 159.
153 X. Y. Chen, H. R. Hu, B. Liu, M. H. Qiao, K. N. Fan and H. Y. He, *J. Catal.*, 2003, **220**, 254.
154 X. Y. Chen, S. Wang, J. H. Zhuang, M. H. Qiao, K. N. Fan and H. Y. He, *J. Catal.*, 2004, **227**, 419.
155 H. Li, J. Liu, H. X. Yang and H. X. Li, *Chin. J. Chem.*, 2009, **27**, 2316.
156 H. Li, Y. Xu, H. X. Yang, F. Zhang and H. X. Li, *J. Mol. Catal. A: Chem.*, 2009, **307**, 105.
157 A. Fukuoka, Y. Sakamoto, S. Guan, S. Inagaki, N. Sugimoto, Y. Fukushima, K. Hirahara, S. Iijima and M. Ichikawa, *J. Am. Chem. Soc.*, 2001, **123**, 3373.
158 M. W. Wang, F. Y. Li and R. B. Zhang, *Catal. Today*, 2004, **93–95**, 603.
159 H. Li, H. X. Li and J. F. Deng, *Appl. Catal., A*, 2000, **193**, 9.
160 H. Li, H. X. Li, W. L. Dai and J. F. Deng, *Appl. Catal., A*, 2001, **207**, 151.
161 Z. Q. Xiong, Z. T. Mi and X. W. Zhang, *Catal. Commun.*, 2007, **8**, 571.
162 H. S. Chung, C. S. H. Chen, R. A. Kremer and J. R. Boulton, *Energy Fuels*, 1999, **13**, 641.
163 J. J. Zou, Z. Q. Xiong, X. W. Zhang, G. Z. Liu, L. Wang and Z. T. Mi, *Ind. Eng. Chem. Res.*, 2007, **46**, 4415.
164 J. J. Zou, Z. Q. Xiong, L. Wang, X. W. Zhang and Z. T. Mi, *J. Mol. Catal. A: Chem.*, 2007, **271**, 209.
165 Y. J. Choi, K. W. Cho, B. W. Cho and Y. K. Yeo, *Ind. Eng. Chem. Res.*, 2002, **41**, 5504.
166 Y. F. Ma, W. Li, M. H. Zhang, Y. Zhou and K. Y. Tao, *Appl. Catal., A*, 2003, **243**, 215.
167 Y. F. Ma, M. H. Zhang, W. Li, B. G. Zhang and K. Y. Tao, *Chin. J. Catal.*, 2004, **25**, 973.
168 L. J. Wang, W. Li, M. H. Zhang and K. Y. Tao, *Appl. Catal., A*, 2004, **259**, 185.
169 W. Li, C. Han, W. Liu, M. H. Zhang and K. Y. Tao, *Catal. Today*, 2007, **125**, 278.
170 M. X. Wu, W. Li, M. H. Zhang and K. Y. Tao, *Chin. J. Catal.*, 2007, **28**, 351.
171 P. Sabatier, *Ind. Eng. Chem.*, 1926, **18**, 1005.
172 A. Stanislaus and B. H. Cooper, *Catal. Rev.: Sci. Eng.*, 1994, **36**, 75.
173 K. M. Bratlie, M. O. Montano, L. D. Flores, M. Paajanen and G. A. Somorjai, *J. Am. Chem. Soc.*, 2006, **128**, 12810.
174 M. Zahmakıran, Y. Tobul and S. Özkar, *J. Am. Chem. Soc.*, 2010, **132**, 6541.
175 J. Li, M. H. Qiao and J. F. Deng, *Chem. J. Chin. Univ.*, 2001, **22**, 1022.
176 R. B. Zhang, F. Y. Li, N. Zhang and Q. J. Shi, *Appl. Catal., A*, 2003, **239**, 17.
177 M. H. Yang, R. B. Zhang and F. Y. Li, *Chin. Chem. Lett.*, 2004, **15**, 1230.
178 S. X. Xu, F. Y. Li and R. Z. Wei, *Carbon*, 2005, **43**, 861.
179 H. X. Li and Y. P. Xu, *Mater. Lett.*, 2001, **51**, 101.
180 Q. Y. Cheng, W. Li, M. H. Zhang, N. J. Guan and K. Y. Tao, *Chin. J. Catal.*, 2001, **22**, 326.
181 Y. Ju and F. Y. Li, *J. Nat. Gas Chem.*, 2006, **15**, 313.
182 R. Zhang, F. Li, Q. Shi and L. Luo, *Appl. Catal., A*, 2001, **205**, 279.
183 H. Song, X. C. Wu, H. Y. Wang and F. Li, *Chin. J. Chem. Eng.*, 2011, **19**, 698.
184 S. H. Xie, M. H. Qiao, H. X. Li, W. J. Wang and J. F. Deng, *Appl. Catal., A*, 1999, **176**, 129.
185 J. Struijk and J. J. F. Scholten, *Appl. Catal.*, 1990, **62**, 151.
186 J. Struijk and J. J. F. Scholten, *Appl. Catal., A*, 1992, **82**, 277.
187 J. Struijk, M. Angremond, W. J. M. Regt and J. J. F. Scholten, *Appl. Catal., A*, 1992, **83**, 263.
188 J. Q. Wang, P. J. Guo, S. R. Yan, M. H. Qiao, H. X. Li and K. N. Fan, *J. Mol. Catal. A: Chem.*, 2004, **222**, 229.
189 J. B. Ning, J. Xu, J. Liu and F. Lu, *Catal. Lett.*, 2006, **109**, 175.
190 Z. Liu, S. H. Xie, B. Liu and J. F. Deng, *New J. Chem.*, 1999, **23**, 1057.
191 H. Z. Liu, T. Jiang, B. X. Han, S. G. Liang, W. T. Wang, T. B. Wu and G. Y. Yang, *Green Chem.*, 2011, **13**, 1106.
192 S. C. Liu, Z. Y. Liu, Z. Wang, S. H. Zhao and Y. M. Wu, *Appl. Catal., A*, 2006, **313**, 49.
193 G. Y. Fan, W. D. Jiang, J. B. Wang, R. X. Li, H. Chen and X. J. Li, *Catal. Commun.*, 2008, **10**, 98.
194 S. C. Liu, G. Luo, H. R. Wang, Y. L. Xie, B. J. Yang and M. L. Han, *Chin. J. Catal.*, 2002, **23**, 317.
195 Z. Y. Liu, H. J. Sun, D. B. Wang, S. C. Liu and Z. J. Li, *Chin. J. Chem.*, 2010, **28**, 1927.
196 P. Gallezot, P. J. Cerino, B. Blance, G. Fleche and P. Fuertes, *J. Catal.*, 1994, **146**, 93.
197 M. H. Qiao, S. H. Xie, W. L. Dai and J. F. Deng, *Acta Chim. Sin. (Engl. Ed.)*, 2000, **58**, 904.
198 J. Guo, Y. J. Hou, C. H. Yang, Y. Q. Wang and L. N. Wang, *Mater. Lett.*, 2012, **67**, 151.
199 J. Guo, Y. J. Hou, C. H. Yang, Y. Q. Wang, H. Q. He and W. Li, *Catal. Commun.*, 2011, **16**, 86.
200 H. B. Guo, H. X. Li, Y. P. Xu and M. H. Wang, *Mater. Lett.*, 2002, **57**, 392.
201 Y. D. Wu, H. B. Guo, Y. Wan, M. H. Wang and H. X. Li, *Chin. J. Catal.*, 2004, **25**, 533.
202 A. W. Heinen, J. A. Peters and H. van Bekkum, *Carbohydr. Res.*, 2000, **328**, 449.
203 L. W. Wright, *CHEMTECH*, 1974, 42.
204 I. Toufeili and S. Dziedzic, *Food Chem.*, 1993, **47**, 17.
205 F. Capet, S. Comini, G. Odou, P. Looten and M. Descamps, *Carbohydr. Res.*, 2004, **339**, 1225.
206 H. Li, D. S. Chu, J. Liu, M. H. Qiao, W. L. Dai and H. X. Li, *Adv. Synth. Catal.*, 2008, **350**, 829.
207 H. Li, P. F. Yang, D. S. Chu and H. X. Li, *Appl. Catal., A*, 2007, **325**, 34.
208 E. van Steen and M. Claeys, *Chem. Eng. Technol.*, 2008, **31**, 655.
209 H. Li, P. F. Yang, D. S. Chu and H. X. Li, *Appl. Catal., A*, 2007, **325**, 34.
210 P. Gallezot and D. Richard, *Catal. Rev.: Sci. Eng.*, 1998, **40**, 81.
211 Y. Zhu, L. Tian, Z. Jiang, Y. Pei, S. H. Xie, M. H. Qiao and K. N. Fan, *J. Catal.*, 2011, **281**, 106.
212 Y. Pei, H. R. Hu, J. Fang, M. H. Qiao, W. L. Dai, K. N. Fan and H. X. Li, *J. Mol. Catal. A: Chem.*, 2004, **211**, 243.
213 Y. Pei, J. Fang, H. R. Hu, J. H. Zhuang, K. N. Fan, H. X. Li and M. H. Qiao, *Acta Chim. Sin. (Engl. Ed.)*, 2005, **63**, 289.
214 Y. Pei, J. Q. Wang, Q. Fu, P. J. Guo, M. H. Qiao, S. R. Yan and K. N. Fan, *New J. Chem.*, 2005, **29**, 992.
215 M. Casagrande, L. Storaro, A. Talon, M. Lenarda, R. Frattini, E. Rodríguez-Castellón and P. Maireles-Torres, *J. Mol. Catal. A: Chem.*, 2002, **188**, 133.
216 H. B. Ji, Y. Y. Huang, L. X. Pei and X. D. Yao, *Catal. Commun.*, 2008, **9**, 27.
217 B. Liu, M. H. Qiao, J. F. Deng, K. N. Fan, X. X. Zhang and B. N. Zong, *J. Catal.*, 2001, **204**, 512.
218 B. Liu, M. H. Qiao, J. Q. Wang and K. N. Fan, *Chem. Commun.*, 2002, 1236.
219 Y. J. Hou, Y. Q. Wang, S. Han, Z. T. Mi, W. Wu and E. Z. Min, *Chin. J. Catal.*, 2004, **25**, 149.
220 Y. J. Hou, Y. Q. Wang and Z. T. Mi, *J. Mater. Sci.*, 2005, **40**, 6585.
221 X. Y. Chen, M. H. Qiao and H. Y. He, *Chin. J. Catal.*, 2011, **32**, 325.
222 Z. Y. Ma, L. X. Zhang, R. Z. Chen, W. H. Xing and N. P. Xu, *Chem. Eng. J.*, 2008, **138**, 517.
223 A. Furst, R. C. Berlo and S. Hooton, *Chem. Rev.*, 1965, **65**, 51.
224 A. Robertson, T. Matsumoto and S. Ogo, *Dalton Trans.*, 2011, **40**, 10304.
225 H. L. Wen, K. S. Yao, Y. D. Zhang, Z. M. Zhou and A. Kirschning, *Catal. Commun.*, 2009, **10**, 1207.
226 B. Chen, U. Dingerdissen, J. G. E. Krauter, H. G. J. L. Rotgerink, K. Möbus, D. J. Ostgard, P. Panster, T. H. Riermeier, S. Seebald, T. Tacke and H. Trauthwein, *Appl. Catal., A*, 2005, **280**, 17.
227 D. Gavroy, C. Joly-Vuillemin, G. Cordier, P. Fouilloux and H. Delmas, *Catal. Today*, 1995, **24**, 103.
228 B. Coq, D. Tichit and S. Ribet, *J. Catal.*, 2000, **189**, 117.
229 P. F. Yang, Z. X. Jiang, P. L. Ying and C. Li, *Chin. J. Catal.*, 2007, **28**, 670.

230 M. H. Wang, H. X. Li, Y. D. Wu and J. Zhang, *Mater. Lett.*, 2003, **57**, 2954.
231 H. X. Li, Y. D. Wu, Y. Wan, J. Zhang, W. L. Dai and M. H. Qiao, *Catal. Today*, 2004, **93–95**, 493.
232 H. X. Li, Y. D. Wu, J. Zhang, W. L. Dai and M. H. Qiao, *Appl. Catal., A*, 2004, **275**, 199.
233 J. L. Dallons, G. Jannes and B. Delmon, *Catal. Today*, 1989, **5**, 257.
234 G. D. Yadav and M. R. Kharkara, *Appl. Catal., A*, 1995, **123**, 115.
235 P. Kukula, V. Gabova, K. Koprivova and P. Trtik, *Catal. Today*, 2007, **121**, 27.
236 I. Mochida and K. Sakanishi, *Fuel*, 2000, **79**, 221.
237 Q. Y. Cheng, W. Li, J. Wu, N. J. Guan and K. Y. Tao, *J. Fuel Chem. Technol.*, 2000, **28**, 249.
238 G. L. Parks, M. L. Pease, A. W. Burns, K. A. Layman, M. E. Bussell, X. Wang, J. Hanson and J. A. Rodriguez, *J. Catal.*, 2007, **246**, 277.
239 S. Skrabalak and K. Suslick, *Chem. Mater.*, 2006, **18**, 3103.
240 X. Qi, Q. Shi, W. Chen and R. Zhang, *Chin. J. Catal.*, 2012, **33**, 543.
241 M. L. Hitchman, R. A. Spackman, N. C. Ross and C. Agra, *Chem. Soc. Rev.*, 1995, **95**, 423.
242 J. X. Chen, D. H. Ci, R. J. Wang and J. Y. Zhang, *Appl. Surf. Sci.*, 2008, **255**, 3300.
243 Z. J. Wu, M. H. Zhang, Z. F. Zhao, W. Li and K. Y. Tao, *J. Catal.*, 2008, **256**, 323.
244 E. Furimsky, *Appl. Catal., A*, 2000, **199**, 147; G. W. Huber, S. Iborra and A. Corma, *Chem. Rev.*, 2006, **106**, 4044.
245 J. Zakzeski, P. C. A. Bruijnincx, A. L. Jongerius and B. M. Weckhuysen, *Chem. Rev.*, 2010, **110**, 3552.
246 W. Y. Wang, Y. Q. Yang, J. G. Bao and H. A. Luo, *Catal. Commun.*, 2009, **11**, 100.
247 W. Y. Wang, Y. Q. Yang, H. A. Luo and W. Y. Liu, *Catal. Commun.*, 2010, **11**, 803.
248 W. Y. Wang, Y. Q. Yang, H. A. Luo and W. Y. Liu, *React. Kinet., Mech. Catal.*, 2010, **101**, 105.
249 W. Y. Wang, Y. Q. Yang, H. A. Luo, H. Z. Peng, X. Z. Zhang and T. Hu, *Chin. J. Catal.*, 2011, **32**, 1645.
250 W. Y. Wang, Y. Q. Yang, H. A. Luo, H. Z. Peng and F. Wang, *Ind. Eng. Chem. Res.*, 2011, **50**, 10936.
251 W. Wang, Y. Yang, H. Luo, T. Hu and W. Liu, *Catal. Commun.*, 2011, **12**, 436.
252 W. Wang, Y. Yang, H. A. Luo, T. Hu and W. Liu, *React. Kinet., Mech. Catal.*, 2011, **102**, 207.
253 W. Wang, Y. Yang, H. Luo, H. Peng, B. He and W. Liu, *Catal. Commun.*, 2011, **12**, 1275.
254 B. Sun, M. H. Qiao, K. N. Fan, J. Ulrich and F. Tao, *ChemCatChem*, 2011, **3**, 542.
255 A. Y. Khodakov, W. Chu and P. Fongarland, *Chem. Rev.*, 2007, **107**, 1692.
256 B. N. Zong, E. Z. Min, S. Z. Dong and J. F. Deng, *Acta Chim. Sin. (Engl. Ed.)*, 1989, **47**, 1052.
257 C. X. Xiao, Z. P. Cai, T. Wang, Y. Kou and N. Yan, *Angew. Chem., Int. Ed.*, 2008, **47**, 746.
258 N. Yan, C. X. Xiao and Y. Kou, *Coord. Chem. Rev.*, 2010, **254**, 1179.
259 X. B. Fan, Z. Y. Tao, C. X. Xiao, F. Liu and Y. Kou, *Green Chem.*, 2010, **12**, 795.
260 X. B. Fan, N. Yan, Z. Y. Tao, D. Evans, C. X. Xiao and Y. Kou, *ChemSusChem*, 2009, **2**, 941.
261 Y. Wang, H. L. Wu, Q. H. Zhang and Q. H. Tang, *Microporous Mesoporous Mater.*, 2005, **86**, 38.
262 X. F. Cheng, B. S. Wu, H. W. Xiang and Y. W. Li, *Chin. J. Catal.*, 2010, **31**, 579.
263 X. F. Cheng, B. S. Wu, Y. Yang, H. W. Xiang and Y. W. Li, *J. Mol. Catal. A: Chem.*, 2010, **329**, 103.
264 R. Datta and M. Henry, *J. Chem. Technol. Biotechnol.*, 2006, **81**, 1119.
265 R. D. Cortright, M. Sanchez-Castillo and J. A. Dumesic, *Appl. Catal., B*, 2002, **39**, 353.
266 G. Luo, S. R. Yan, M. H. Qiao and K. N. Fan, *Appl. Catal., A*, 2007, **332**, 79.
267 G. Y. Fan, Y. Zhang, Y. F. Zhou, R. X. Li, H. Chen and X. J. Li, *Chem. Lett.*, 2008, 852.
268 F. H. A. Bolder, *Ind. Eng. Chem. Res.*, 2008, **47**, 7496.
269 R. J. Shi, F. Wang, Tana, Y. Li, X. M. Huang and W. J. Shen, *Green Chem.*, 2010, **12**, 108.
270 K. Oded, S. Musa, D. Gelman and J. Blum, *Catal. Commun.*, 2012, **20**, 68.
271 S. Sato, R. Takahashi, T. Sodesawa and F. Nozaki, *J. Catal.*, 1997, **169**, 447.
272 B. Rajesh, N. Sasirekha and Y. W. Chen, *Ind. Eng. Chem. Res.*, 2007, **46**, 2034.
273 W. Fang, Q. Zhang, J. Chen, W. Deng and Y. Wang, *Chem. Commun.*, 2010, **46**, 1547.
274 M. Hayashi, K. Yamada, S. Nakayama, H. Hayashi and S. Yamazaki, *Green Chem.*, 2000, **2**, 257.
275 T. Mitsudome, Y. Mikami, H. Funai, T. Mizugaki, K. Jitsukawa and K. Kaneda, *Angew. Chem., Int. Ed.*, 2008, **47**, 138.
276 M. Bertoli, A. Choualeb, A. J. Lough, B. Moore, D. Spasyuk and D. G. Gusev, *Organometallics*, 2011, **30**, 3479.
277 B. Rajesh, N. Sasirekha and Y. W. Chen, *J. Mol. Catal. A: Chem.*, 2007, **275**, 174.
278 B. Rajesh, N. Sasirekha, S. P. Lee, H. Y. Kuo and Y. W. Chen, *J. Mol. Catal. A: Chem.*, 2008, **289**, 69.
279 A. Biabani-Ravandi and M. Rezaei, *Chem. Eng. J.*, 2012, **184**, 141.
280 Z. X. Ding, H. Y. Yang, J. F. Liu, W. X. Dai, X. Chen, X. X. Wang and X. Z. Fu, *Appl. Catal., B*, 2011, **101**, 326.
281 Q. Miao, G. Xiong, S. Sheng, W. Cui, L. Xu and X. Guo, *Appl. Catal., A*, 1997, **154**, 17.
282 J. H. Ryu, K. Y. Lee, H. J. Kim, J. I. Yang and H. Jung, *Appl. Catal., B*, 2008, **80**, 306.
283 F. Mudu, B. Arstad, E. Bakken, H. Fjellvåg and U. Olsbye, *J. Catal.*, 2010, **275**, 25.
284 K. Li, H. Wang, Y. Wei and D. Yan, *Chem. Eng. J.*, 2011, **173**, 574.
285 M. A. Peña, J. P. Gómez and J. L. G. Fierro, *Appl. Catal., A*, 1996, **144**, 7.
286 L. Chen, Y. Lu, Q. Hong, J. Lin and F. M. Dautzenberg, *Appl. Catal., A*, 2005, **292**, 295.
287 Z. L. Ma, R. L. Jia, C. J. Liu and Z. T. Mi, *Chem. Lett.*, 2002, 884.
288 Z. L. Ma, R. L. Jia and C. J. Liu, *J. Mol. Catal. A: Chem.*, 2004, **210**, 157.
289 R. L. Jia, Z. L. Ma, C. Y. Wang and S. M. Wang, *React. Kinet. Catal. Lett.*, 2005, **85**, 73.
290 Y. Wang, J. S. Zhang, X. C. Wang, M. Antonietti and H. R. Li, *Angew. Chem., Int. Ed.*, 2010, **49**, 3356.
291 V. Z. Fridman and A. A. Davydov, *J. Catal.*, 2000, **195**, 20.
292 H. Z. Liu, T. Jiang, B. X. Han, S. G. Liang and Y. X. Zhou, *Science*, 2009, **326**, 1250.
293 L. Zhuang, H. X. Li, W. L. Dai and M. H. Qiao, *Chem. Lett.*, 2003, 1072.
294 J. L. Liu, H. Li and H. X. Li, *Chin. J. Catal.*, 2007, **28**, 312.
295 H. Li, J. L. Liu and H. X. Li, *Mater. Lett.*, 2008, **62**, 297.
296 M. G. Davie, M. Reinhard and J. R. Shapley, *Environ. Sci. Technol.*, 2006, **40**, 7329.
297 M. G. Davie, K. Shih, F. A. Pacheco, J. O. Leckie and M. Reinhard, *Environ. Sci. Technol.*, 2008, **42**, 3040.
298 S. Takaç, B. Akay and T. H. Özdamar, *Enzyme Microb. Technol.*, 1995, **17**, 445.
299 Y. P. Chao, Z. J. Lai, P. Chen and J. T. Chern, *Biotechnol. Prog.*, 1999, **15**, 453.
300 G. X. Li, L. Li, H. M. Huang and H. Q. Cai, *J. Mol. Catal. A: Chem.*, 2003, **193**, 97.
301 C. M. Hayward, D. Yohannes and S. J. Danishefsky, *J. Am. Chem. Soc.*, 1993, **115**, 9345.
302 R. E. Estévez, J. Justicia, B. Bazdi, N. Fuentes, M. Paradas, D. Choquesillo-Lazarte, J. M. García-Ruiz, R. Robles, A. Gansäuer, J. M. Cuerva and J. E. Oltra, *Chem.–Eur. J.*, 2009, **15**, 2774.
303 T. D. Haddad, L. C. Hirayama and B. Singaram, *J. Org. Chem.*, 2010, **75**, 642.
304 C. J. Li and T. H. Chan, *Tetrahedron Lett.*, 1991, **32**, 7017.
305 H. Li, F. X. Dong, M. W. Xiong, H. X. Li, P. Li and X. G. Zhou, *Adv. Synth. Catal.*, 2011, **353**, 2131.
306 F. Tao and M. Salmeron, *Science*, 2011, **331**, 171.
307 M. A. Bañares, *Adv. Mater.*, 2011, **23**, 5293.
308 B. N. Zong, *Catal. Surv. Asia*, 2007, **11**, 87.
309 R. E. Rosensweig, *Science*, 1979, **204**, 57.
310 Z. Y. Pan, M. H. Dong, X. K. Meng, X. X. Zhang, X. H. Mu and B. N. Zong, *Chem. Eng. Sci.*, 2007, **62**, 2712.

